



*Research article*

## **Øysand research site: Geotechnical characterisation of deltaic sandy-silty soils**

**Santiago Quinteros<sup>1,3,\*</sup>, Aleksander Gundersen<sup>1</sup>, Jean-Sebastien L’Heureux<sup>2</sup>, J. Antonio H. Carraro<sup>3</sup> and Richard Jardine<sup>3</sup>**

<sup>1</sup> Offshore Geotechnics, Norwegian Geotechnical Institute, Sognsveien 72, N-0855 Oslo, Norway

<sup>2</sup> Geotechnics and Natural Hazards Trondheim, Norwegian Geotechnical Institute, Høgskoleringen 9, N-7034 Trondheim, Norway

<sup>3</sup> Department of Civil and Environmental Engineering, Imperial College London, Skempton Building, South Kensington Campus, SW7 2AZ, London, UK

\* **Correspondence:** Email: [santiago.quinteros@ngi.no](mailto:santiago.quinteros@ngi.no); Tel: +4740100376.

**Abstract:** This paper describes the geology and geotechnical engineering properties of the fluvial and deltaic gravelly-sandy-silty sediments at Øysand, Norway. Geophysical and geotechnical site investigations carried out between 2016 and 2018 at the site are presented. Field testing included state-of-the-practice and state-of-the-art soil characterisation techniques such as total sounding, seismic cone penetration testing, seismic flat dilatometer, multichannel analysis of surface waves, electrical resistivity tomography, ground penetrating radar, piezometers, thermistors strings, slug tests, and permeability tests using a newly developed CPT permeability probe from NGI. Several sampling techniques were used at the site to assess sample quality. Laboratory testing consisted of index tests and advanced triaxial tests with bender elements to estimate shear strength and stiffness. Data interpretation, engineering soil properties and state variables derived from this analysis are presented, along with comments on data quality. Engineering problems investigated at Øysand so far and discussed in this paper are related to: the impact of using different CPTU types, sample quality assessment by obtaining soils with state-of-the-practice and state-of-the-art techniques (such as gel-push sampler and ground freezing), and frost heave susceptibility.

**Keywords:** gravelly sand; silt; *in situ* testing; sampling; laboratory testing; site characterization; permeability

---

## 1. Introduction

The research presented in this paper integrates with the Norwegian Geo-Tests Sites (NGTS) project [1], the purpose of which is the development and characterisation of five geotechnical test sites in Norway: a silty sand site at Øysand (this article), a silt site at Halden [2], a soft clay site at Onsøy [3], a quick clay site at Tiller/Flotten [4] close to Trondheim (see Figure 1) and a permafrost site in Longyearbyen, Svalbard [5]. This paper presents the characterisation of the Øysand site.

Silty sand deposits are common in many parts of the world, including rivers, offshore banks and deltaic areas, where many major cities are constructed. Intrinsic properties and state variables affect soil behaviour [6]. Intrinsic properties include mineralogy, particle angularity and surface roughness, gradation (including grain size distribution and its derivatives such as fines content), etc. State variables include relative density ( $D_r$ ), mean effective stresses ( $p'$ ), fabric, overconsolidation ratio (OCR) and the coefficient of earth pressure at rest ( $K_0$ ), and may relate to cementation and ageing. State-of-the-art techniques for characterization and sampling have been applied to estimate the *in situ* soil properties at Øysand. The derived intrinsic and engineering parameters obtained from the field and laboratory testing are summarized in this paper. A link is presented between the geological history and its impact on the engineering parameters, as established through *in situ* and laboratory testing. The geotechnical knowledge acquired at the Øysand research site will contribute to expanding the current understanding of the engineering behaviour of natural silty sandy deposits.

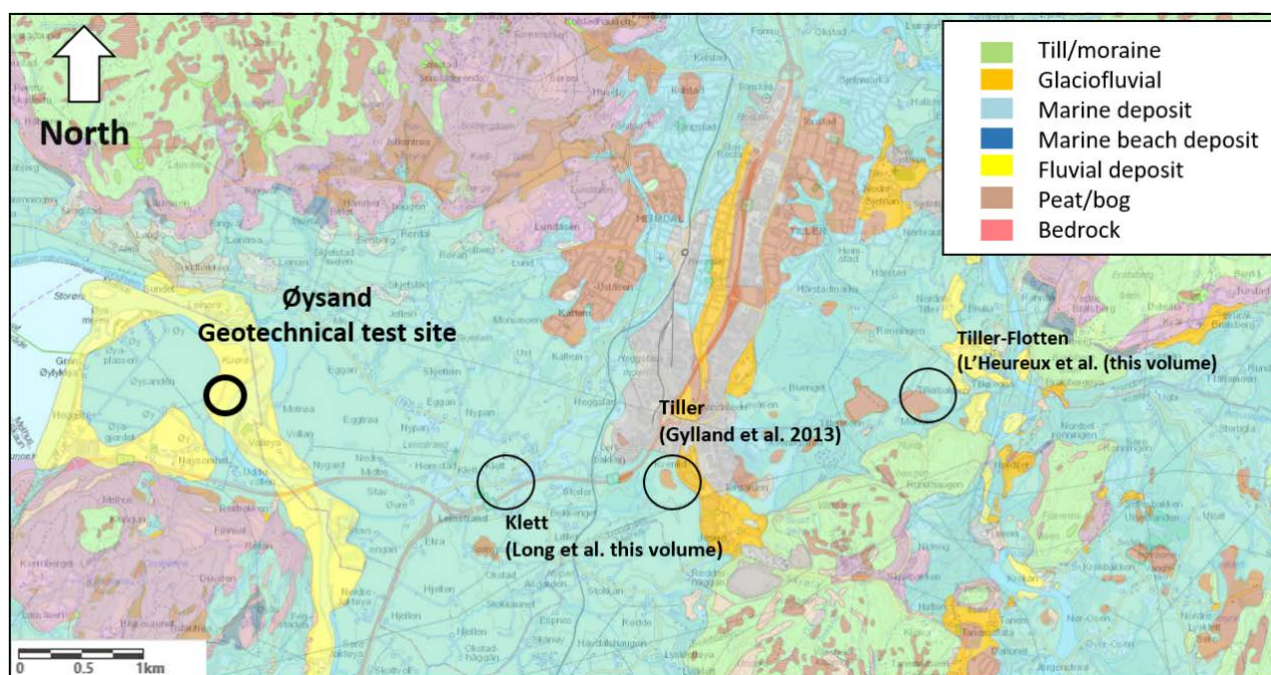


**Figure 1.** Geological map of Øysand peninsula (data from: [www.ngu.no](http://www.ngu.no)).

## 2. Regional setting

The Øysand site is located about 15 km south-west from Trondheim, Norway (see Figure 2). The sand deposit at Øysand originates from the Gaula River, a 150 km long river with an average discharge of  $97 \text{ m}^3/\text{s}$  which flows into the Trondheimsfjord and borders the site to the east, see Figure 2.

An area of approximately 35,000 m<sup>2</sup>, that is used mainly for agricultural purposes, is available for geotechnical investigations at Øysand. The deposit at the site consist of fluvial material, underlain by deltaic and marine sediments (Figure 2). While the depth to bedrock is unknown, a 1940s investigation made during the German occupation of Norway showed that the sediments extend to a depth of at least 80 m below ground level.

The site topography comprises a practically flat surface that reposes around 2.7 m above sea level, with the exception of a 7 m high ridge along the south part of the field. A road enables access throughout the year. Two farms are located about 500 m south-west of the site.

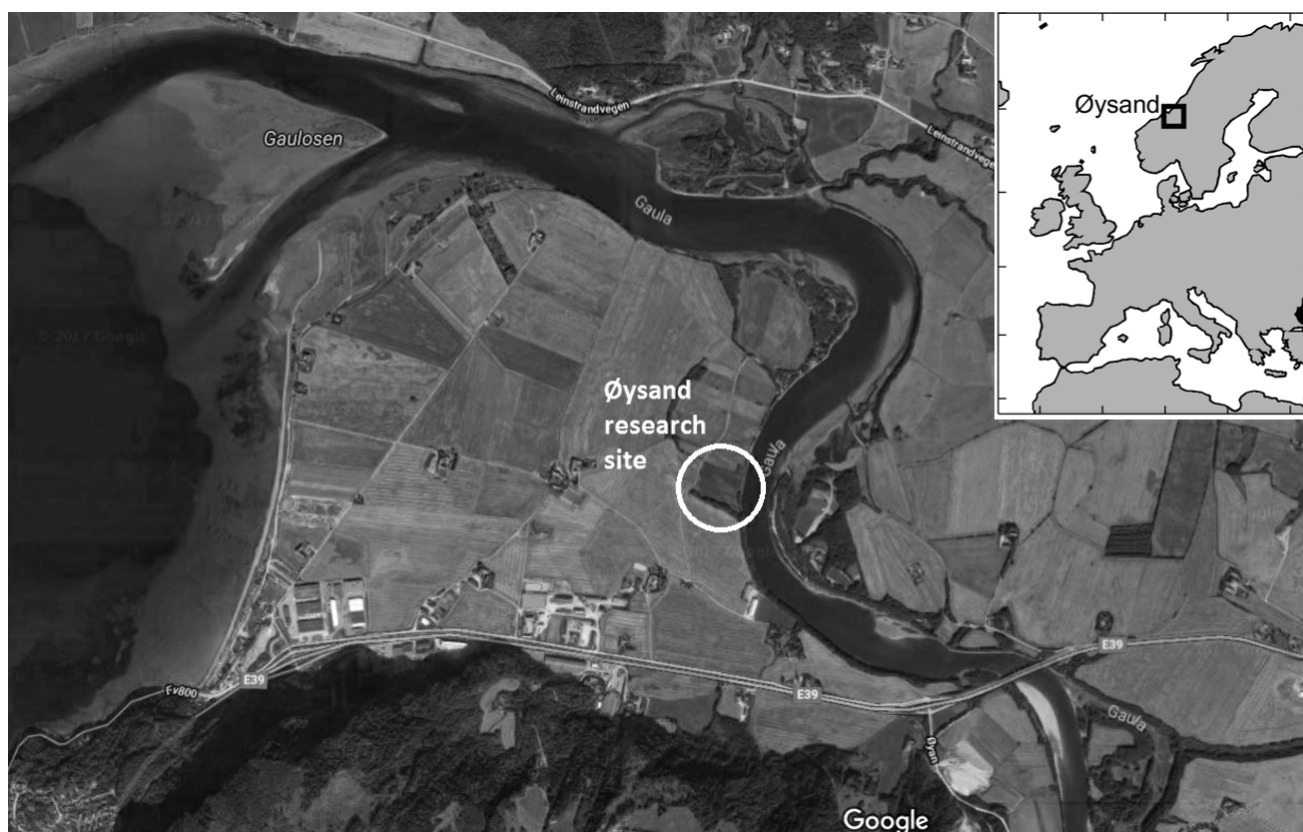


**Figure 2.** Location of the Øysand research site (modified from *Google Maps* 2017).

### 3. Overview of field and laboratory data

Site characterization at the Øysand research facility started in 2016 as part of the Norwegian GeoTest site project (NGTS). A wide range of *in situ* tools, geophysical techniques, sampling techniques and laboratory tests have been used to assess the geological history and geotechnical properties of the sand deposits since 2016. A complete list of all geotechnical work, geophysical investigations, and laboratory tests performed at the site (including tests procedures, references and derived geotechnical parameters) is given in Table 1. The field test locations are shown in Figure 3.

Site characterization at Øysand has involved geophysical and geotechnical techniques. Geophysical tests included: Multichannel Analysis of Surface Waves (MASW), Symmetrical Resistivity Profiling (SRP), Multi-Sensor Core Logging (MSCL), Electrical Resistivity Tomography (ERT), Ground Penetration Radar (GPR) and Self Polarization (SP). Geotechnical tests included:

Total Soundings (TS), Cone Penetration Tests (CPTU), Seismic Cone Penetration Test (SCPTU), Seismic Dilatometer Tests (SDMT), Piezometers (Piezo), Thermistors Strings (THS), Slug test (SLU), and Permeability tests using a NGI newly developed permeability probe [7]. Soil was sampled using the Sonic Drill Sampler (SDS), the Geonor Push Piston Sampler (GPP), an open Push Piston Sampler (PPS), and the Japanese Gel-Push Sampler (GPS). Sampling with an *in situ* ground freezing technique was conducted in April and May of 2019.

MSCL results are used for indirect estimation of the water content ( $w$ ) and unit weight ( $\gamma$ ) of the soil. ERT and GPR results were used for interpretation of a 3D geological map of the site and for preliminary assessment of soil layering. ERT and GPR results were also used during the sampling campaigns for identifying the thickest layers of sand for specifying the sampling locations. CPT and DMT results are used for soil classification and for indirect estimation of *in situ*  $\gamma$ ,  $D_r$  and  $K_0$ . Ground temperature was measured using THS. Permeability was obtained from Slug tests and the NGI permeability probe, respectively, and the results were compared with laboratory tests. Field and laboratory measurements of shear wave velocity from MASW/SCPTU/SDMT and Bender elements (BE) are used for estimating the small strain shear modulus ( $G_{max}$ ).

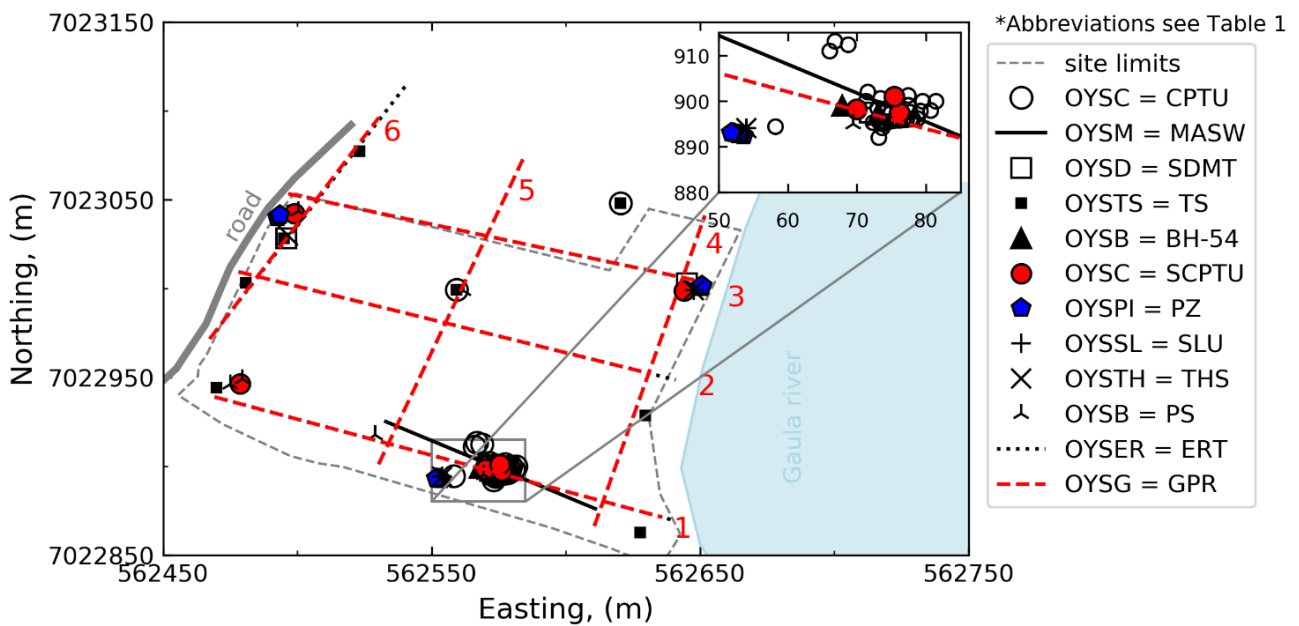


**Figure 3.** Location of field tests at Øysand research site.

**Table 1.** Summary of geophysical, *in situ* and laboratory tests performed at Øysand.

Test	Abbreviation	Measured/Controlled	Interpreted	Reference/Comment
<i>Geophysical/non-intrusive</i>				
Electrical resistivity tomography (ERT)	OYSER	Resistivity	$Z_{\text{bedrock}}$ , soil type	by NGI <sup>1</sup>
Ground penetration radar (GPR)	OYSG	$F_{\text{DT}}$	$Z_{\text{bedrock}}$	by NGI
Multi-channel analysis of surface waves (MASW)	OYSM	$v_p$ , $\omega$	$v_s$ , $G_{\text{max}}$	by APEX <sup>2</sup> , and Reykjavik University
<i>In situ</i>				
Total sounding (TS)	OYSTS			
Cone penetration test (CPTU, SCPT)	OYSC	$q_c$ , $f_s$ , $u_2$ , $v_{s,vh}$	$\sigma'_p$ , $G_{vh,max}$ , $\phi'$	
Seismic flat dilatometer (SDMT)	OYSD	$P_0$ , $P_1$ , $I_D$ , $K_D$ , $E_D$ , $v_{vh}$	$K_0$ , $\sigma'_p$ , $\phi'$	
Piezometers (PZ)	OYSPI	$u$ , $t$	$u_0$	Pore pressure
Thermistor string (THS)	OYSTH	$T$ , $t$	-	
Slug tests (SLU)	OYSSL	Pressure head	$k$	
NGI permeability probe (NGI-flow cone)	OYSC	Flow	$k$	
<i>Sampling</i>				
Geonor fixed piston composite (PS $\varnothing$ 54 mm)	OYSB_PS54	-	-	2 BH, 12 tubes
Thin wall push piston sampler (PS, $\varnothing$ 72 mm)	OYSB_PS72	-	-	4 tubes
Gel-Push Sampler (GPS, $\varnothing$ 72 mm)	OYSB_GPS	-	-	2 tubes
Ground freezing ( $\varnothing$ 100 mm)	OYSB_GF	-	-	April & May 2019
<i>Laboratory</i>				
Water content	-	$w$	-	
Unit weight (density)	-	$\gamma_d$ , $\gamma_t$ ( $\rho_d$ , $\rho_t$ )	-	
Unit weight of solid particles	-	$\gamma_s$	-	
Grain size distribution	-	-	% gravel, sand, silt, clay	
Multi sensor core logging (MSCL)	-	$\rho$ , MS	N	NGU in-house <sup>3</sup>
Split core imaging	-	-	-	NGU in-house
Hydraulic conductivity	-	$k_v$	$k_v$	
Triaxial test: CAUC, CADC	-	$\varepsilon_a$ , $\varepsilon_r$ , $\varepsilon_p$ , $u$ , $p$ , $q$	$\phi'_{cs}$ , $\phi'_p$ , $E$	
Bender element test (BE)	-	$v_{s,vh}$	$G_{vh,max}$	
Micro computed tomography (CT)	-	-	-	On each tube and specimen

<sup>1</sup> NGI = Norwegian Geotechnical Institute, Oslo Norway<sup>2</sup> APEX = Apex Geoservices, Wexford, Ireland<sup>3</sup> NGU = Geological Survey of Norway, Trondheim, Norway (in Norwegian: Norges Geologiske Undersøkelse)

## 4. Engineering geology

### 4.1. Deglaciation history and depositional environment

Following deglaciation of the region approximately 10,300 years ago, the study area was subject to glacio-isostatic rebound and fall of relative sea-level. The highest relative sea level of the Øysand area is approximately 175 m.a.s.l. above the current sea level [8]. Throughout the Holocene the mouth of the Gaula River continuously moved in a north-westwards direction in phase with delta progradation. The coarser deltaic and fluvial sediments deposited directly on the seafloor which consisted mostly of silts and clays (marine deposits). A quaternary geology map of the study presented in Figure 1 shows that the entire research site is located on a fluvial deposit reposing on thick deposits of marine clays.

According to the shoreline regression curve for the region [9], the study area probably emerged from the sea only about 1000–1500 years ago. As a consequence, the deltaic sediments at Øysand are fairly young. Following their emergence from the sea, the deltaic deposits were covered by coarser river deposits as the Gaula River meandered in the valley. Coarse sands and gravels are therefore expected to occur in the upper portion of the soil stratigraphy at Øysand.

### 4.2. Source of material

The catchment area of the Gaula river is 3668 km<sup>2</sup> and is dominated by rocks from the Caledonian mountain range, including greenstone, amphibolite, tuff, and micaceous shales [10]. The deposits found at Øysand today were produced by glacial erosion of the bedrock and fluvial erosion of marine and glacial deposits in the catchment. The major mineralogical components of the bedrock and glacial deposits in the catchment area are quartz, feldspars, illite and chlorite with the latter making up the main proportion of the clay fraction.

### 4.3. Hydrological conditions and stress history

A total of 12 electrical piezometers (Geotech PVT with built-in data loggers) were installed in clusters around the site. Their depths range from 5 to 20 m below ground level. One cluster was installed near the Gaula River (OYSPI06–OYSPI10), second cluster (OYSPI01–OYSPI05) is located 160 m to 170 m away from the river in the southern part of the study area, and a third one (OYSPI11–OYSPI12) close to the access road (see Figure 3). The piezometers reveal that the ground water level (GWL) is generally set around 2 m below ground level. Pore pressure measurements taken from May to December of 2017 are shown in Figure 4a with time. Figure 4b shows that the groundwater pressure increases hydrostatically with depth. However, locations near to the river are also affected by neap and spring tides from the nearby Trondheimsfjord, which occur every month and generate cyclic variations of about  $\pm 10$  kPa in the pore pressures and hence vertical and horizontal effective stresses.



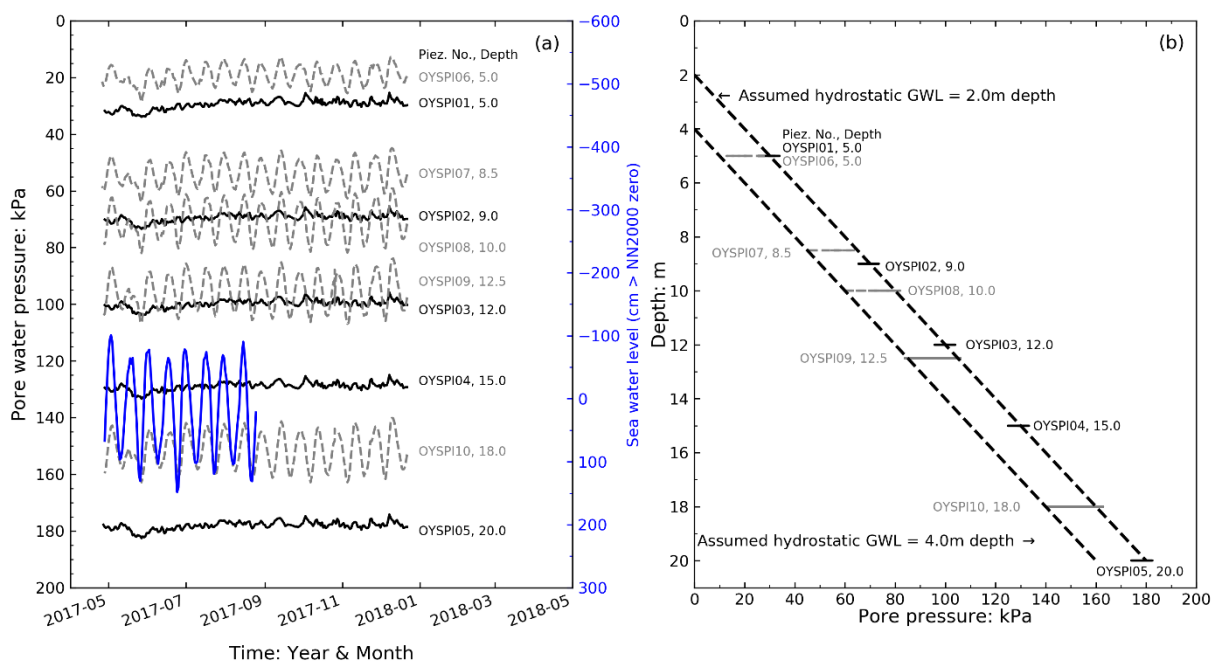


**Figure 4.** Piezometer results: (a) pore pressure with time, (b) pore pressure with depth.

The 7 m high ridge located in the south of the study area was most likely formed by erosion as the Gaula River meandering across the area (Figure 5). Any such erosion of overlying sediments would have left the sands encountered today in an overconsolidated condition. No other previous loading processes have been identified to date.

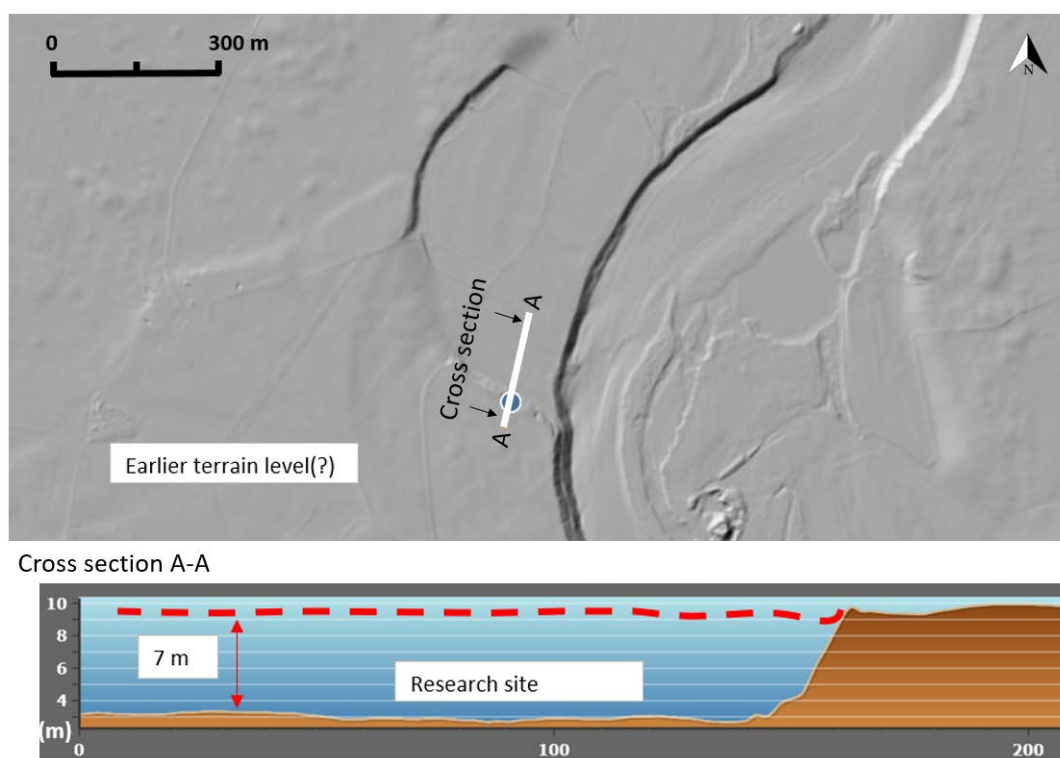








**Figure 5.** Possible erosion of the site by the Gaula River (data from: [www.hoydedata.no](http://www.hoydedata.no)).

#### 4.4. Stratigraphy

The stratigraphy at the site has been interpreted on the basis of *in situ* soundings, boreholes logs and geophysical data. Due to its geological history, the soil deposit at Øysand presents several layers and significant lateral variability. In general, the stratigraphy down to 20 m below ground surface can be divided into two main units: i) a top 6–10 m of coarse to gravelly sand (fluvial deposit), and ii) a lower unit consisting mostly of fine silty sand (deltaic soils), see also [11]. The lower unit also presents layers of clay and silt. Photographs of typical soil samples at the site, and a description of the soil, are presented in Table 2. Figure 6 shows the material from OYSB09 in the south of the Øysand site. Figure 7 shows a complete borehole log down to 20 m below ground level.

A combined geophysical survey consisting of ERT and GPR was carried out in April 2017. A total of 6 profiles were recorded, exact locations are illustrated in Figure 3. ERT is useful for obtaining 2D and/or 3D maps of the spatial and temporal variation of the soil electrical conductivity, which also correspond to variations in soil water content [12], grain size and pore water chemistry.

**Table 2.** Summary of Øysand stratigraphy, with photos of selected samples.

Depth range [m]	Soil description [-]	Image [-]
0.0–2.0	SAND, silty, fine, loose to medium dense, with organic material	
2.0–10.0	SAND, fine to coarse gravelly, medium dense, with layers of fine to medium silty sand and traces of organic material	 
10.0–20.0	Depending on the location: Either, SAND, fine to medium silty with thick layers of SILT, sandy, clayey material, medium dense to dense. Or, SAND, fine to medium silty with thin traces of silty sandy material, medium dense	  

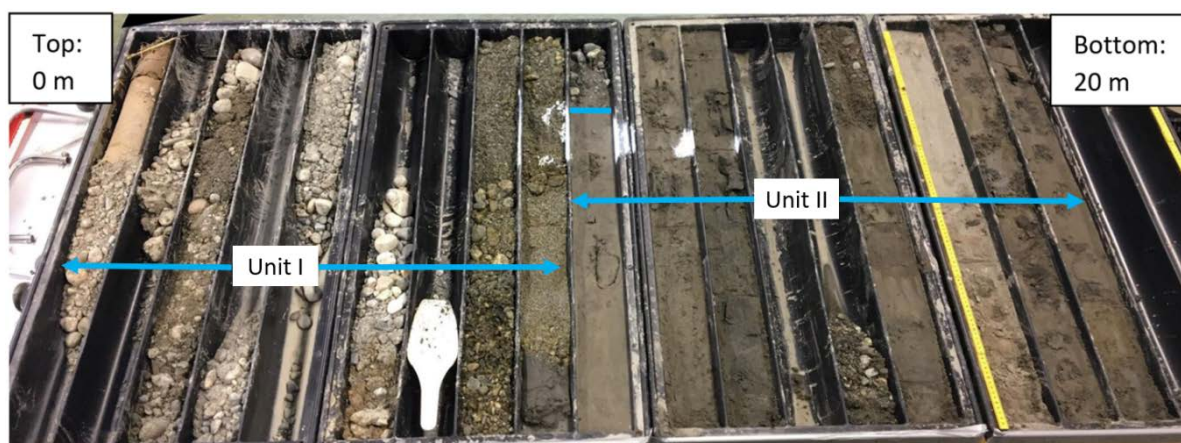


**Figure 6.** Stratigraphy based on soil sampled towards the south of site (OYSB09).



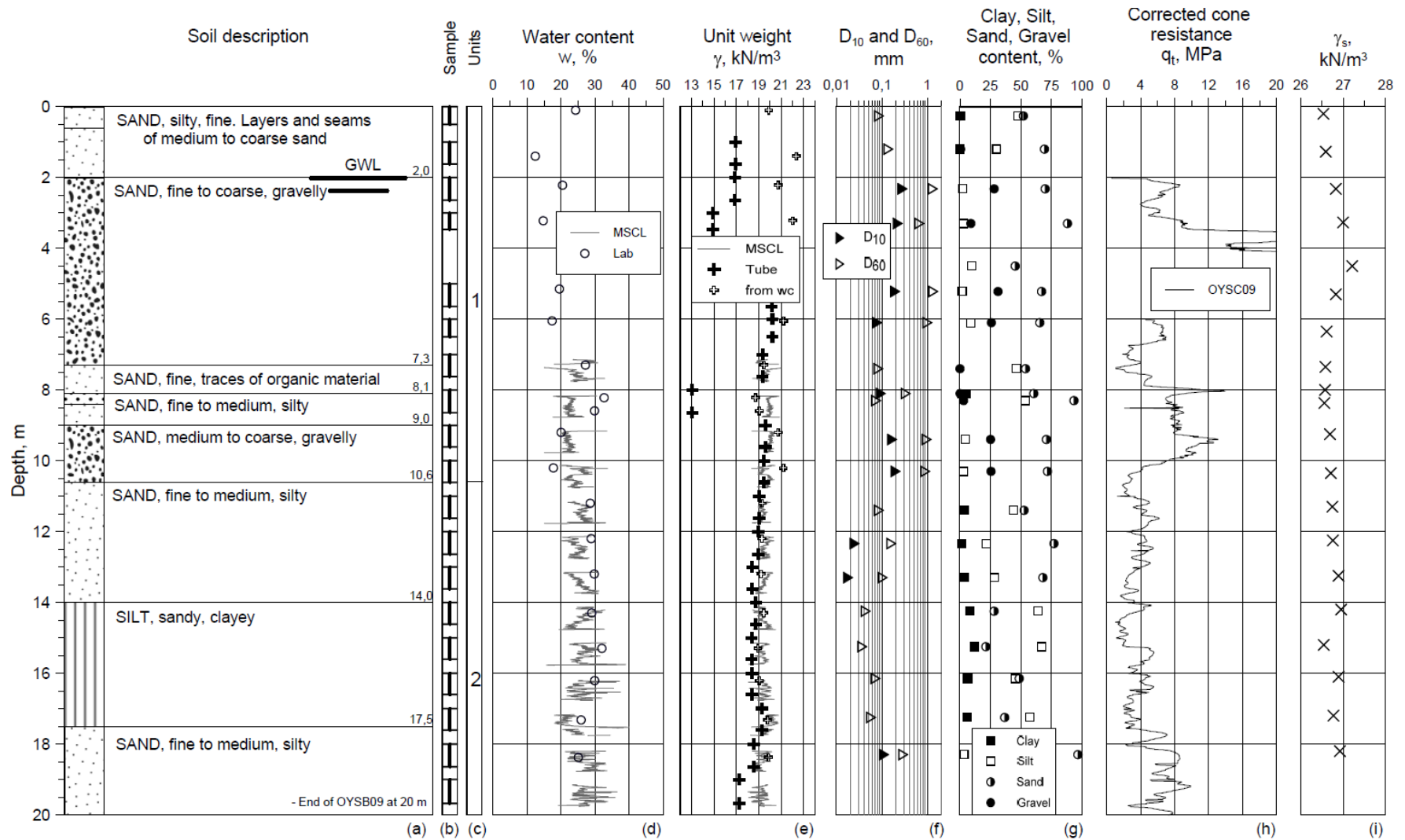


**Figure 7.** Borehole log (OYSB09). \* Multi sensor Core Logging, \*\*  $q_t = q_c + u_2(1 - a)$  after [13].

ERT results are presented in Figure 8. They show a generally consistent higher resistivity layer down to 10 m below the terrain, which corresponds to the upper coarse to gravelly sand (Unit I). Below this, resistivity decreases gradually from around 250  $\Omega\text{m}$  down to 50  $\Omega\text{m}$  in the lower Unit II of silty fine sand. The gradual change in resistivity may be linked to the coarsening upward found in this unit.

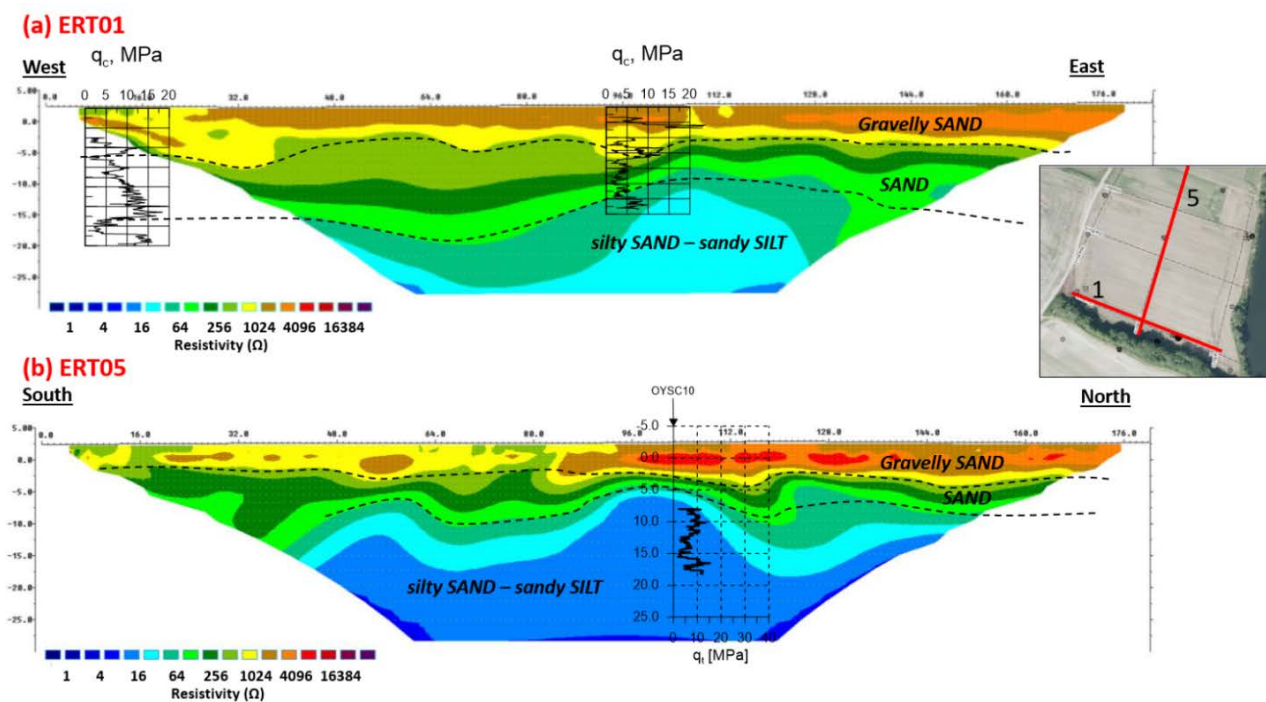


**Figure 8.** ERT interpretation: (a) ERT01 and (b) ERT05.

Due to the rapid attenuation of electromagnetic waves in the deposit, GPR data provides shallower information than the ERT (down to approximately 6–7 m). Results shown in

Figure 9 indicate multiple reflections around 2 m below ground surface. This may correspond to the top of the gravelly soil, but might also be influenced by the groundwater level. Below this the GPR data reflects several layers dipping in a north-westward direction, following the likely direction of delta progradation and the deltaic fore sets.

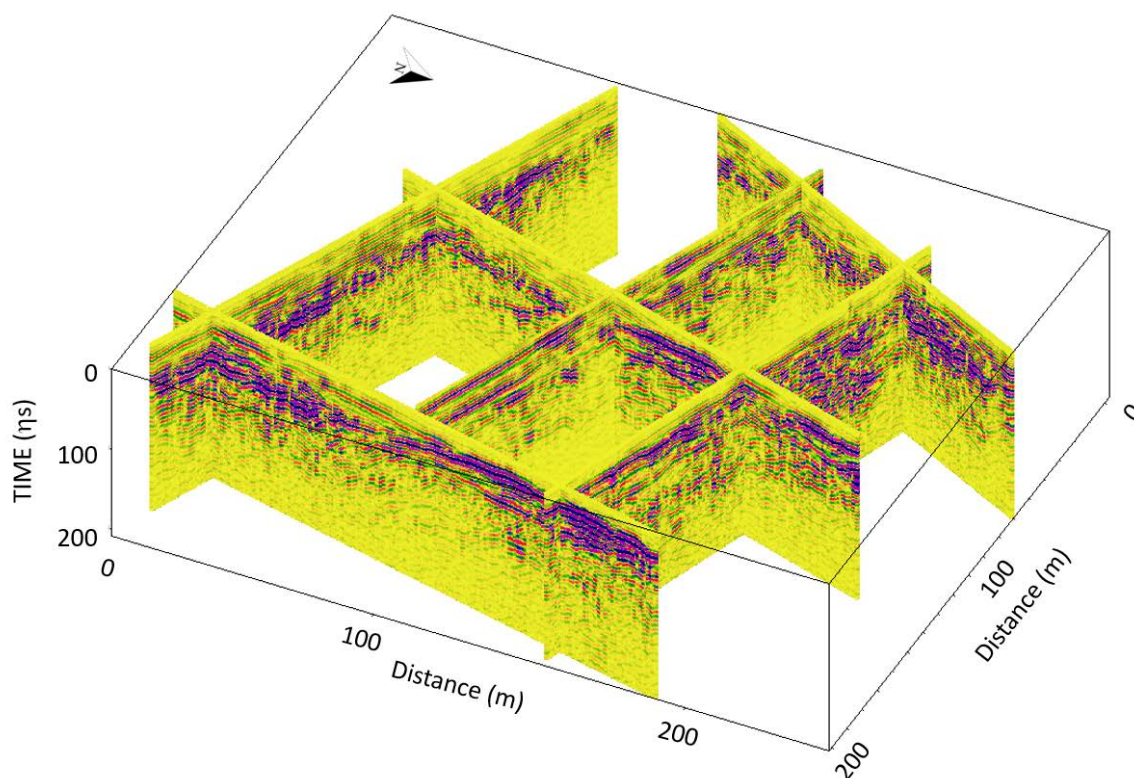


**Figure 9.** GPR interpreted 3D model.

## 5. Soil composition

### 5.1. Grain size distribution

Representative grain size distribution (GSD) curves obtained from OYSB09 samples are presented in Figure 10a. The fine to coarse sandy gravelly soil of Unit I from about 0 m to 10 m depth (mostly classified as well-graded sand (SW after [14]) and the sandy silty layers of soil from Unit II from about 10 m to 20 m depth (classified as silty sand, silt and poorly graded sand (SM, ML and SP after [14]) are represented in this figure. The fines content (particles  $<0.06$  mm) ranges from 2% to 80%, depending on the soil layer of interest. A classification triangle is given in Figure 10b, showing that the sandy/silty Øysand soils do not contain significant amounts of clay. Fines content is also presented in Figure 13c.

Values of  $D_{10}$  and  $D_{60}$  are shown in Figure 7f. Values of  $D_{10}$  are as low as about 0.02 mm and as high as 1 mm for  $D_{60}$ . Higher values of  $D_{60}$  and  $D_{10}$  are found in the upper layers of Unit I, while lower values are found in Unit II. The variations with depth of the amounts of gravel, sand, silt and clay, by percentage, are shown in Figure 7g. In Unit I, the gravel content varies between 5% and 50% while the sand content varies between 50% and 90%. In the same unit, the silt content is generally low, usually less than 10% (though some thin layers may have up to 50% silt), and no clay is observed. In Unit II, no gravel content is observed, while the sand contents vary from 25% to 75%. For this same unit, the silt content varies from 25% to 75% while the maximum clay content was below 15% (in the silt layer).

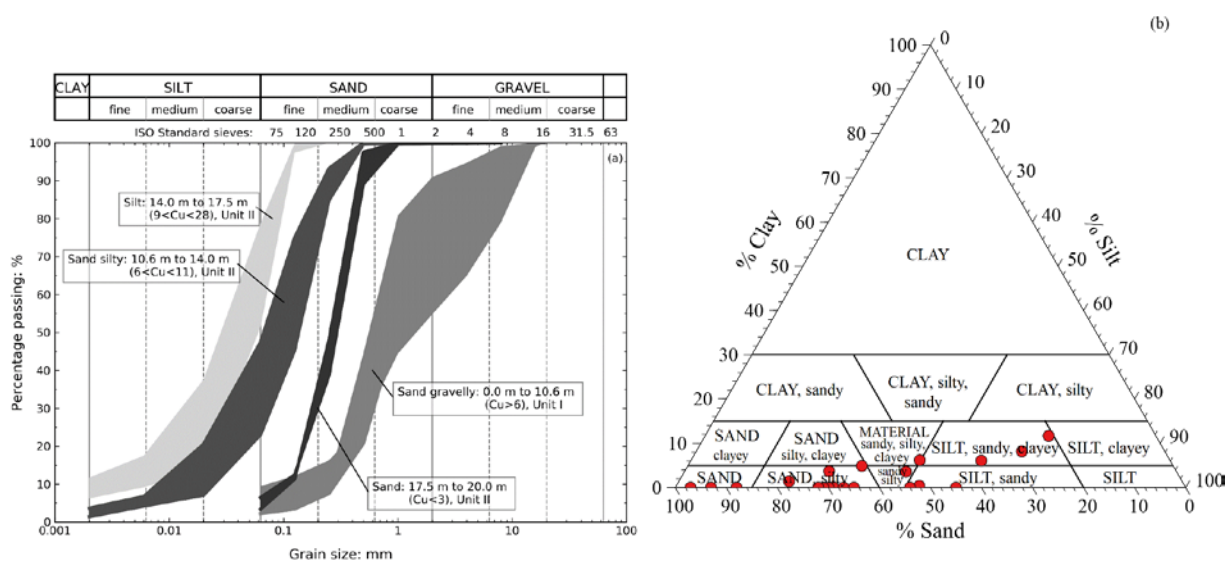


**Figure 10.** (a) Grain size distributions at Øysand from OYSB09, (b) classification triangle.

## 5.2. Grain angularity

Particle angularity and sphericity were assessed for gravelly sand samples from 2.5 to 3.6 m depth, using an optical microscope. According to the terminology outlined by [15], Øysand sand particles are mainly sub-rounded and have high sphericity. Detailed results are presented in Table 3. A computed tomography (CT) image from the shallow sand is shown in Figure 11. Note that the grain angularity of the silt layers will be determined in a later stage, using a scanning electron microscope (SEM).

**Table 3.** Angularity and sphericity (after [15]).

Angularity (from a total of 642 particles observed)						Sphericity	
Very angular	Angular	Sub-angular	Sub-rounded	Rounded	Well-rounded	Low	High
3%	13%	28%	39%	16%	1%	40%	60%

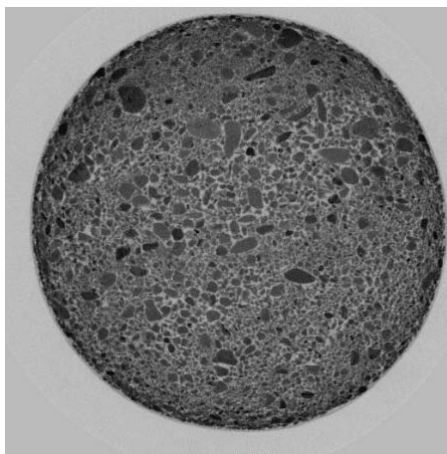


**Figure 11.** Micro CT scan of shallow gravelly sand 2.5 to 3.6 m depth (from OYSB09).

### 5.3. Soil fabric

Unit II is generally non-homogeneous, mottled, with primary bedding and laminations depending on the depth of the layer. Micro CT scans of the main types of fabric observed are presented in Figure 12. In Figure 12a a randomly distributed gravelly material in a sandy silty matrix is observed at 14.5 m depth, whereas distinctive layers of gravel and silty sand are shown in Figure 12b at 15.4 m depth. Figure 12c shows the primary inclination of the silty soil from about 16.7 m depth, with typical inclination angles of up to about 25°.

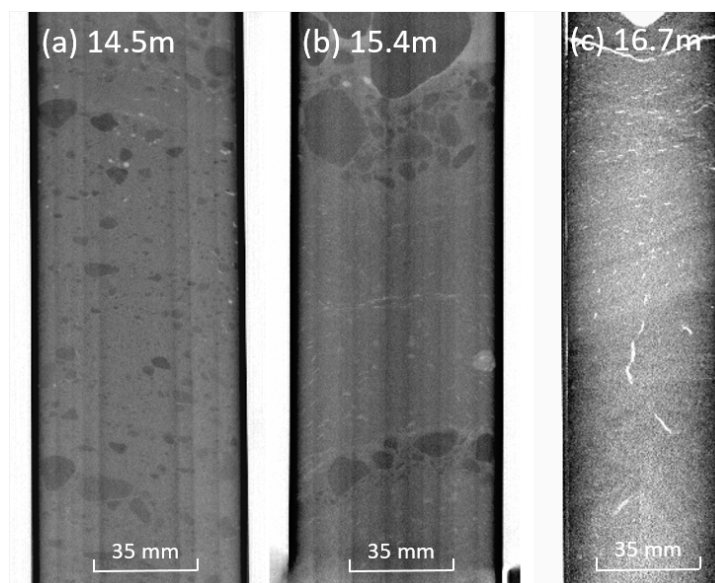


**Figure 12.** CT-scans of soil at (a) 14.0 m depth, (b) 15.4 m and 16.7 m depth (from OYSB09).

## 6. Index parameters

### 6.1. Water content

Water contents,  $w$ , were determined using two methods: (i) by oven drying soil samples, and (ii) from multi-sensor core logging. The results summarised in Figure 7 show  $w$  increasing from between 10–20% in the unsaturated part of the coarse gravelly sand unit, to values close to 30% in the silty sand of Unit II. Measurements of water content in the gravelly sand layers of Unit I are more scattered than in the samples below 11 m, because water tend to segregate within the tubes towards the bottom of the tube during transportation, handling and storage. MSCL readings are only available from 7.3 m depth and below, results are somehow comparable to the obtained with the method (i). An average of  $w = 28\%$  is estimated for Unit II.

### 6.2. Unit weight of solid particles

Values of the unit weight of solid particles ( $\gamma_s$ ), determined according to [16], are shown in Figure 7i. In Unit I,  $\gamma_s$  varies between 26.5 kN/m<sup>3</sup> to 27.2 kN/m<sup>3</sup>, while in Unit II  $\gamma_s$  is between 26.6 kN/m<sup>3</sup> to 26.9 kN/m<sup>3</sup>. An average value of 26.7 kN/m<sup>3</sup> is assumed for Unit II (specific gravity,  $G_s = 2.7$ ).



### 6.3. Bulk or total unit weight

Total unit weight ( $\gamma$ ) was obtained by three different methods: (a) directly from measurements of the weight and volume from piston liners filled with sampled soil, (b) indirectly from water content measurements of the samples and assuming full saturation (reasonable below the ground water level, GWL), and (c) estimated from MSCL readings from 7.2 m to 20 m depth. The unit weight obtained from (a) is less reliable in Unit I soils, because during the sampling process loose material may tend to contract, while dense layers may dilate. As seen in Figure 7e, measurements of  $\gamma$  in the first 7 m depth are quite scattered, low values of unit weight were derived from PPS tubes (between  $14 \text{ kN/m}^3$  and  $17 \text{ kN/m}^3$ ) and high values from water content were obtained ( $20 \text{ kN/m}^3$  to  $22 \text{ kN/m}^3$ ). The high variability of unit weight in the upper layers is questioned due to the mentioned sampling issues. In general, the unit weight at OYSB09 ranges between ca.  $18 \text{ kN/m}^3$  and  $20 \text{ kN/m}^3$  from 5 m to 20 m depth. A representative profile of  $19 \text{ kN/m}^3$  can be assumed for the entire site.

### 6.4. Indirect estimation of *in situ* relative density

Figure 13a shows the results of  $\gamma_{d,\max}$  and  $\gamma_{d,\min}$ , obtained using the NGI method [17]. NGI  $\gamma_{d,\min}$  uses a tube with inner diameter equal 35 mm to place the dry sample in a mould of 72 mm in diameter. As seen in this figure, values of  $\gamma_{d,\max,\text{NGI}}$  and  $\gamma_{d,\min,\text{NGI}}$  change significantly with depth, reflecting the change in particle size distribution at Øysand site. Values of  $\gamma_d$  obtained from  $\gamma$  and the water content as described above are also shown in Figure 13a. Values of  $D_r$  determined after four methods are given in Figure 13b, namely a) based on  $\gamma_d$  from the liner tubes, b) from water contents of PPS samples, c) from extruded and trimmed specimens from the PS liners, and d) from CPTU data using [18]. Note that  $D_r$  values for the sandy/silty soil from CPTU fall below 40% (from 10 m to 20 m depth), while higher values are determined from the other measurements. For reference, the fines content is also presented in Figure 13c. For depths below 11m depth, the relative density based on water content estimation, or direct measurements of weight and volume from sampled soil is significantly higher than the empirically estimated  $D_r$  values using CPTU data. The disturbance induced during the sampling process may have caused the soil to increase its density, hence the values of  $D_r$  based on a) b) and c) methods may exceed the *in situ* values. However,  $D_r$  estimates derived from CPTU data through calibration chamber tests (such as those reported by [18] on air-pluviated, freshly deposited, uniform, clean (zero fines) normally-consolidated silica sands might also be misleading for the natural Øysand soils. It is estimated that the average relative density of the investigated Øysand soils falls around 60%, with some locally looser soil layers presenting 30% relative density. More exact values of  $D_r$  will be acquired from future testing of samples obtained in April and May 2019 by a ground freezing technique.

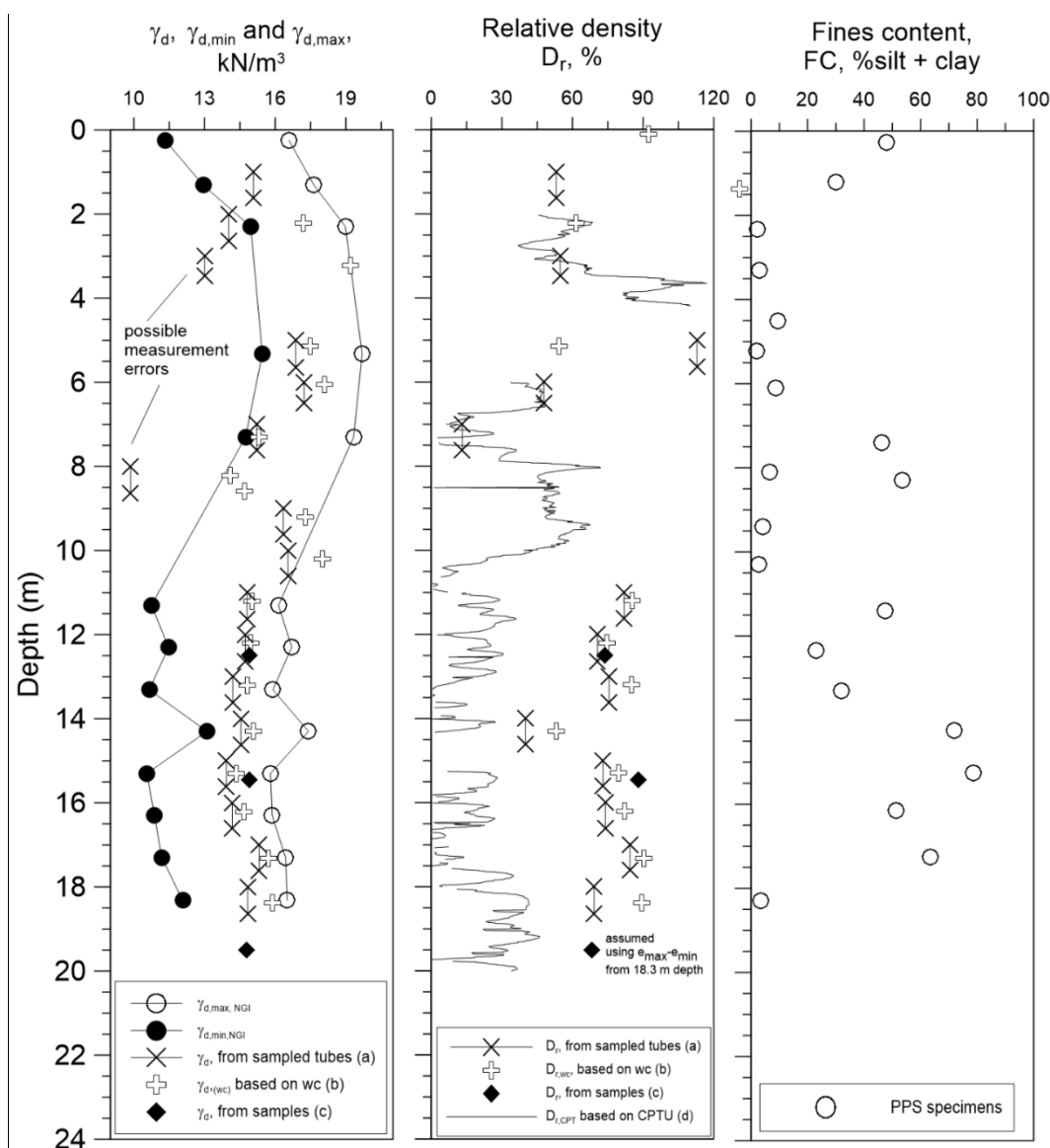


**Figure 13.** (a) Dry unit weight, maximum and minimum unit weights, (b) relative density, and (c) fines content (from OYSB09).

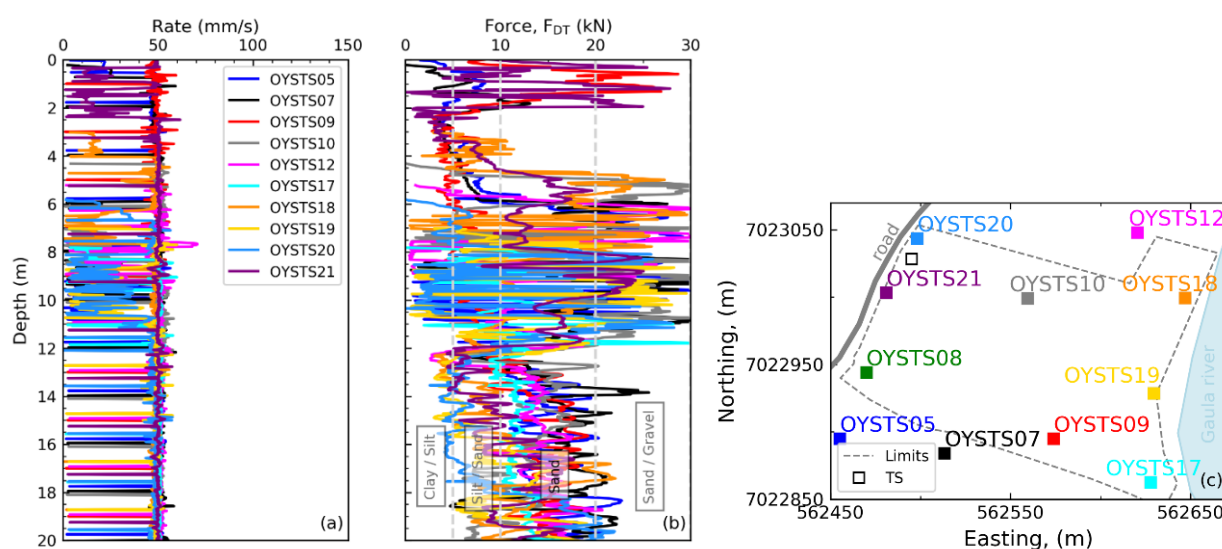
## 7. *In situ* testing

Several *in situ* and advanced laboratory tests were performed to determine the engineering parameters of the Øysand site, as listed in Table 1. In this section, the measured *in situ* data is presented first, followed by comparisons of the derived engineering properties from both field and laboratory tests. The presented data focus on the silty sandy materials encountered in Unit II.

### 7.1. Total sounding (TS)

Total sounding is a static-to-dynamic penetration test method used widely in Scandinavia to determine stratification in soils and to determine the depths to solid ground or bedrock. Test procedures and equipment are described in [19]. The results provide a basis for identifying soils and

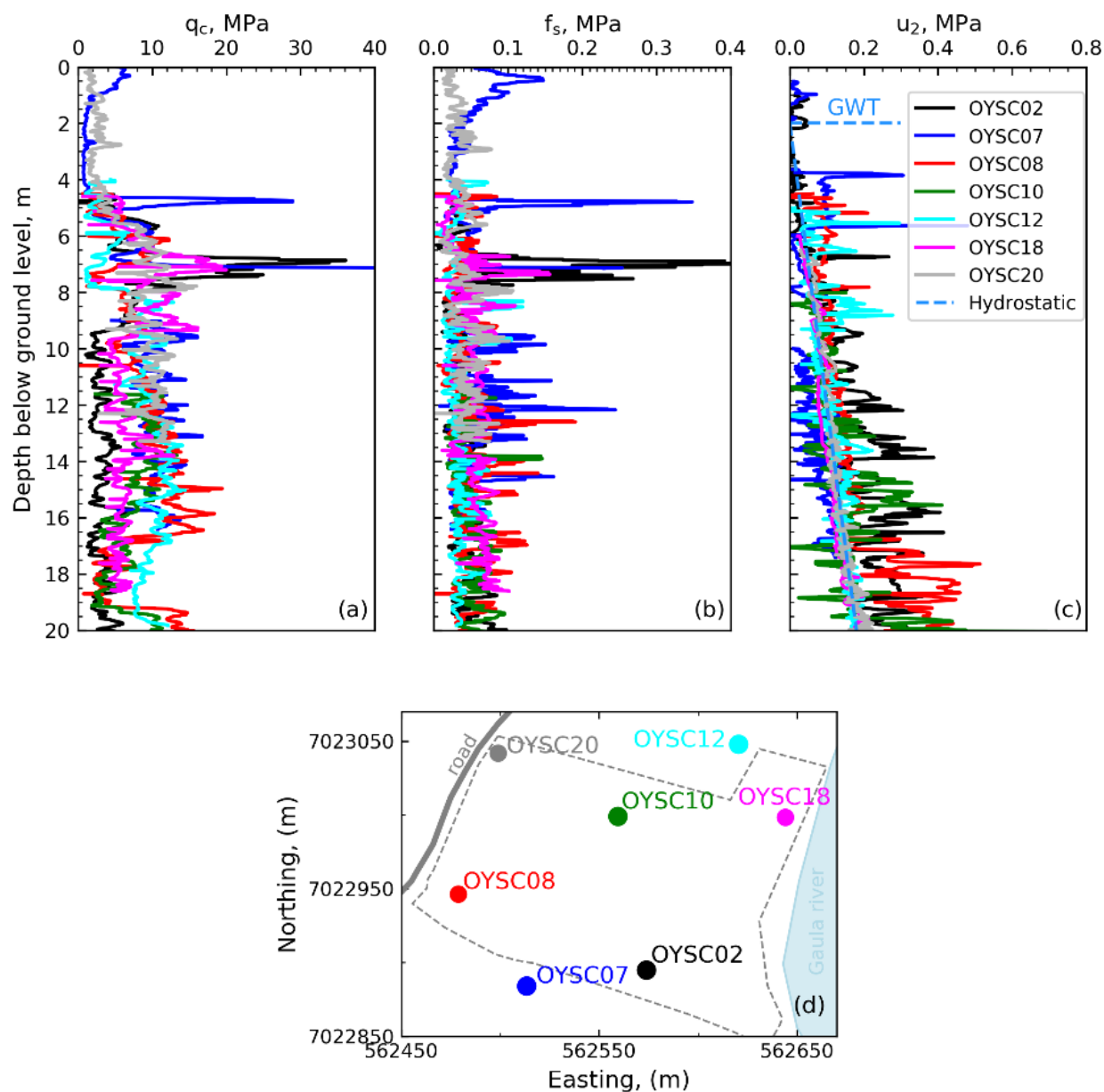
assessing their relative *in situ* shear strengths, following the procedures described in [19]. Results of all TS tests are summarized in Figure 14. Note that the depths of the TS have been adjusted to focus on the main layers identified across the site. The stiff gravelly layer of variable thickness is observed throughout the site. Hammering and flushing were required to advance through sections of this layer. At locations OYSTS08 and OYSTS09 this layer was mostly penetrable with little hammering, but application of forces in excess of 20 kN was required. At locations OYSTS10 and OYSTS12 similar stiff layers were also encountered. Below this layer softer soils were encountered to at least 20 m depth. The gravelly layers at Øysand are clearly identified when observing Figure 14a. Sandy layers are expected typically below the gravel. Figure 14 provides only an indication of the soil inhomogeneity & variability, and shows qualitatively Unit I (gravelly sand) and Unit II (sandy silty soils).



**Figure 14.** TS tests at Øysand: (a) Drilling rate, (b) force with depth, (c) location plan.

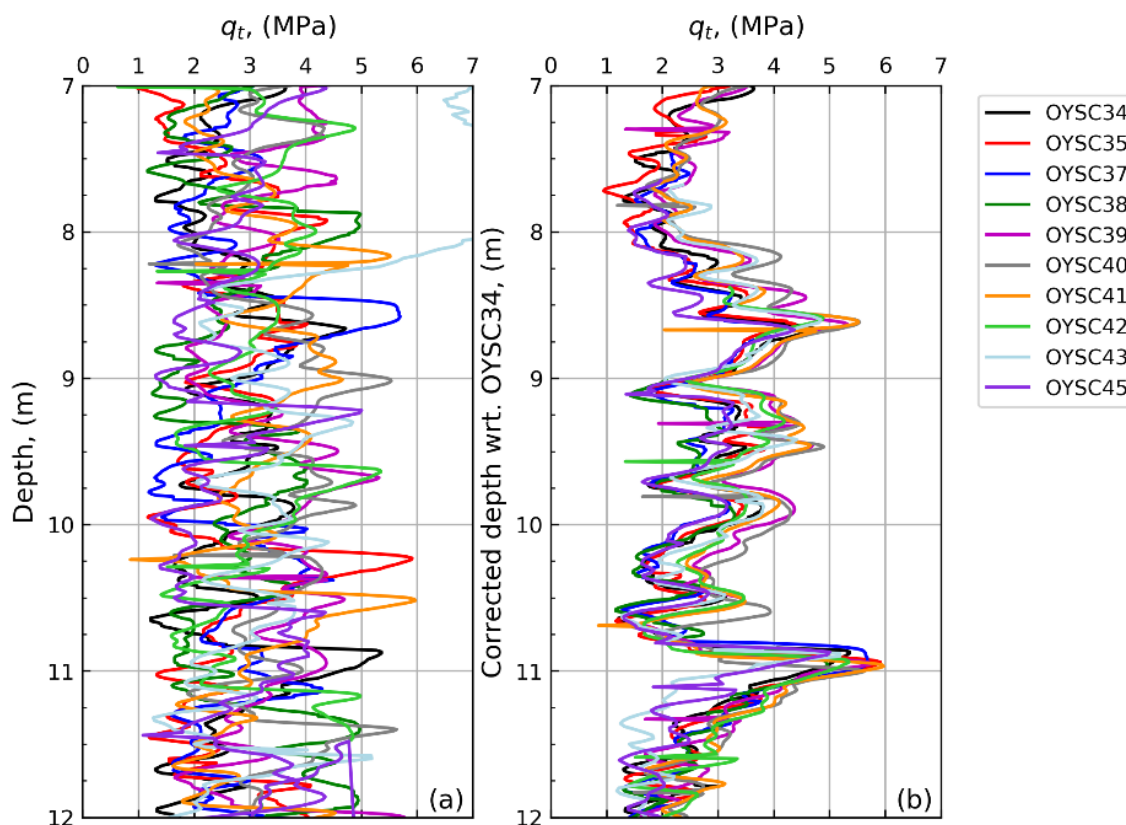
## 7.2. Cone penetration testing (CPTU)

Figure 15 shows CPTU results in terms of cone resistance,  $q_c$ , sleeve friction,  $f_s$ , and pore water pressure,  $u_2$ . The CPTU results presented cover the entire area of the site. A Geotech AB CPTU cone was used for the tests shown in Figure 15. CPTU tests employing cones from other manufacturers have also been carried out (see Section 10.1). Testing was performed following [20]. As seen in Figure 15,  $q_c$ ,  $f_s$ , and  $u_2$  measurements vary considerable with depth and location. Most of the CPTU tests were performed from depths below 4 m to avoid damaging the cones on the top gravelly sand layers. Sand layers seem to be thicker at the locations OYSC07, OYSC08, OYSC12, OYSC18 and OYSC20. More silty soils were encountered at locations OYSC02, OYSC10.



**Figure 15.** CPTUs around the Øysand site perimeter: (a)  $q_c$ , (b)  $f_s$ , (c)  $u_2$  with depth, and (d) location plan.

The variability of the CPTU data per depth shown in Figure 15, is explained by the depositional history of the site. Unit II consist mostly of deltaic foreset beds dipping at an angle up to 20–25°. There is thus a need for a slight depth adjustment to bring the CPTU data into phase, see Figure 16. The depth-wise correction of the CPTUs helps to visualize the homogeneity of the sand layers across the site.



**Figure 16.** CPTU  $q_t$ : (a) uncorrected, (b) corrected depth “in-phase”.

### 7.3. Flat dilatometer (DMT)

Two Marchetti SDMT tests (OYSD09 and OYSD18) were performed about 100 m distance from each other. Testing was done by following [21] guidelines. Results are presented in terms of material index,  $I_D$ , horizontal stress index,  $K_D$ , and dilatometer modulus,  $E_D$ , in Figure 17.  $I_D$ ,  $K_D$  and  $E_D$  are intermediate parameters, which are obtained from the corrected first and second reading,  $p_0$ , and,  $p_1$ , respectively. In turn  $p_0$  and  $p_1$  are obtained from the DMT readings A and B. Reading A is the pressure required to just begin to move the membrane (lift-off pressure), while reading B is the pressure required to expand the membrane centre 1.1 mm against the soil. Details about the equipment, measurements and test interpretation are found in [22].

As seen in Figure 17, sandy silty soils are indicated as predominating at Øysand, with some locally thick layers of silt towards the south of the site. In general, the DMT measurements are compatible with the stratigraphy described in previous sections. A thorough assessment of the DMT ability to estimate the soil type and unit weight at Øysand is found in [11]. Assessment of OCR and  $K_0$  based on DMT is presented in Section 9 of this paper.



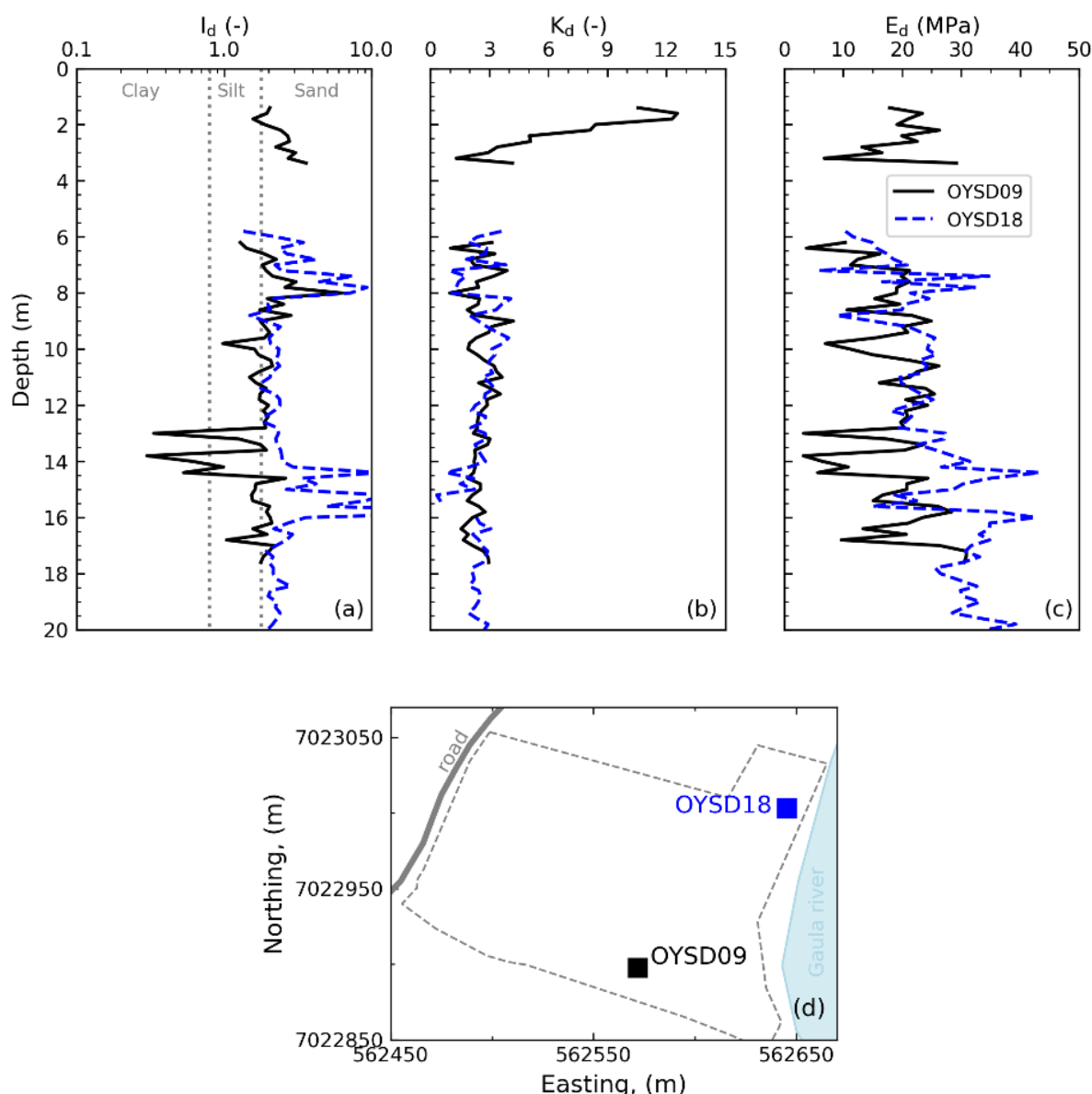


**Figure 17.** DMT results: (a) Material index,  $I_D$ , (b) Horizontal stress index,  $K_D$ , and (c) Dilatometer modulus,  $E_D$  with depth, and (d) location plan.

#### 7.4. Shear wave velocities ( $v_s$ ) and small strain stiffness ( $G_{max}$ )

Direct measurements of  $v_s$  were made using a seismic piezo cone (SCPTU), a seismic dilatometer (SDMT) and MASW. Differences values of  $v_s$  can be obtained due to the different propagation and polarization of the waves. In theory,  $v_s$  measured with SDMT or SDMT propagate vertically and are horizontally polarized ( $v_{s,vh}$ ), while MASW is closer to  $v_{s,hv}$  (horizontally propagating, vertically polarized). Finally, laboratory values of shear waves obtained with bender elements on 54 mm diameter piston samples at NGI, are also presented herein for comparison. Bender element values impose a vertical propagating, horizontal polarized wave  $v_{s,vh}$  as SCPTU or SDMT.

MASW (OYSM01 and OYSM03) profiles were acquired at the same locations where SCPTU (OYSC09, OYSC18 and OYSC20) and SDMT (OYSD01 and OYSD02) were performed. As described in [1], the SCPTU or SDMT configurations had a source at ground level and two geophones inside SCPTU, or geophones inside the SDMT, mounted behind the cone or dilatometer, respectively, with a 0.5 or 1.0 m spacing thus giving a measure of  $v_{s,vh}$ . In order to increase the signal-to-noise ratio on SCPTU readings and reduce the uncoherent noise the seismic traces were typically stacked and filtered through a Butterworth bandpass filter. The velocity was computed from the time lag corresponding to the maximum of the cross-correlation between the two geophone signals. The MASW data acquisition was conducted using a linear array of 24 vertical geophones with a natural frequency of 4.5 Hz, and the inversion of the dispersion curves provided a 1D shear wave velocity,  $v_{s,hv}$ , profile averaging the subsurface properties below the geophone array.

Parallel tests conducted at locations OYSC09, OYSD01, and OYSM01 allow the various types of measurements to be compared directly. In general, all  $v_s$  values vary with the soil layering and depths, as shown in Figure 18. The profile in Figure 18a shows scattered values of  $v_{s,SDMT}$  in the upper gravelly sand layers between 0 m and 1 m depth. Measurements of  $v_s$  from SCPTU and SDMT do not match well as  $v_{s,SCPTU}$  is usually higher than  $v_{s,SDMT}$ . MASW values of  $v_{s,MASW}$  fall in between SCPTU and SDMT results down to about 18 m depth, below that depth MASW results follow the SDMT trend. Note that three different interpretations, by three different engineers, were applied on the MASW data.

Figure 18b shows interpreted  $G_{max}$  values made from the  $v_s$  measurements presented in Section 7.4 by assuming unit weights, isotropic elasticity and fixed Poissons ratios. These  $G_{max}$  estimates vary between about 40 MPa and 100 MPa. The scatter of  $G_{max}$  in the gravelly sand of the first 4 m reflects the scatter of  $v_s$  measurements and the difficulty of determining  $\gamma$  in those shallow layers.  $G_{max}$  differences between the SCPTU and SDMT derived values naturally follow the same trends as  $v_s$ . A significant variation of  $G_{max}$  is observed ( $\pm 50$  MPa), which is not only attributed to the inherent scatter of the soil, but also to the method used (SCPTU, SDMT, MASW, BE) and geometry of wave polarization. Differences between SDMT and SCPTU can also arise due to the different interpretation methods used while post-processing the data. Moreover, the horizontal and vertical variability of the soil and anisotropy in both fabric and *in situ* stress conditions may generate direction-dependent elastic stiffnesses that also contribute to the discrepancy of the values (see [23,24]), so that a direct comparison with depth is not strictly possible. Additionally, not all tests were carried out simultaneously, hence changes in the GWL may also lead to small changes in  $v_s$ .

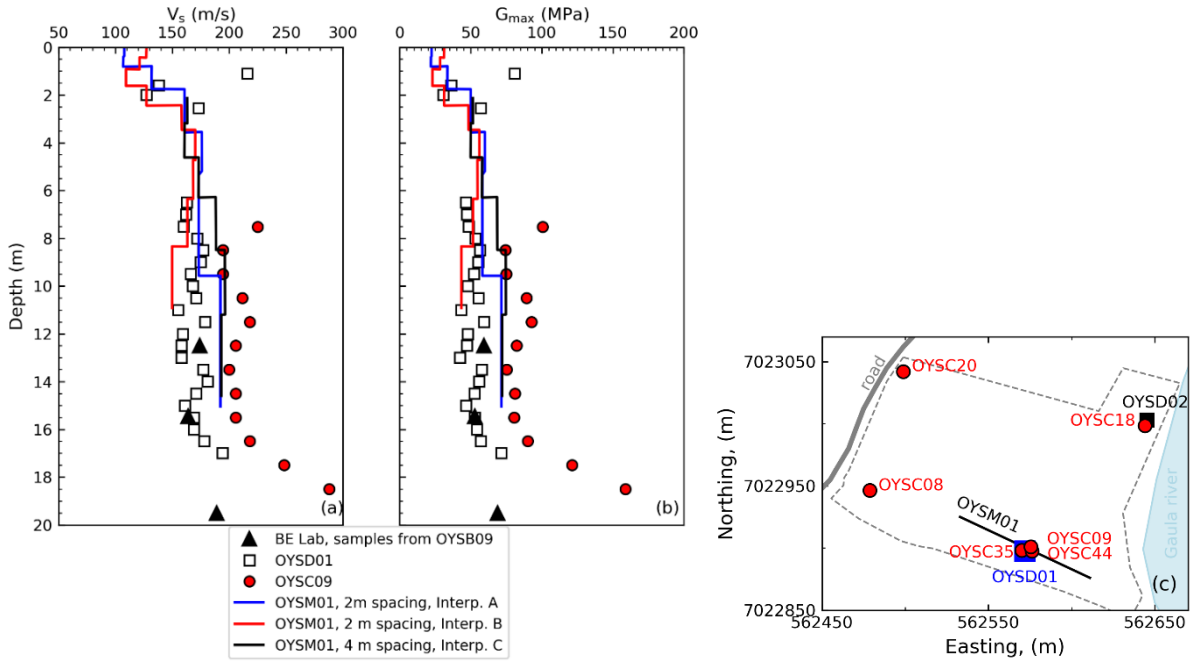


**Figure 18.** (a)  $v_s$  and (b)  $G_{max}$  with depth, (c) location plan.

7.5. Permeability ( $k$ )

Permeability was assessed by several methods including: (i) slug tests (falling head) on boreholes OYSB04 and OYSB03, (ii) a newly developed permeability cone by NGI [7] at OYSC62 location, (iii) estimates from grain size distribution from soil samples obtained on borehole OYSB09, and (iv) from laboratory tests on 54-mm Geonor push piston samples and on OYSB09 samples. The coordinates of the mentioned locations are shown in Figure 19. As seen in this figure, tests were performed far apart from each other and soil variability probably influenced the results.

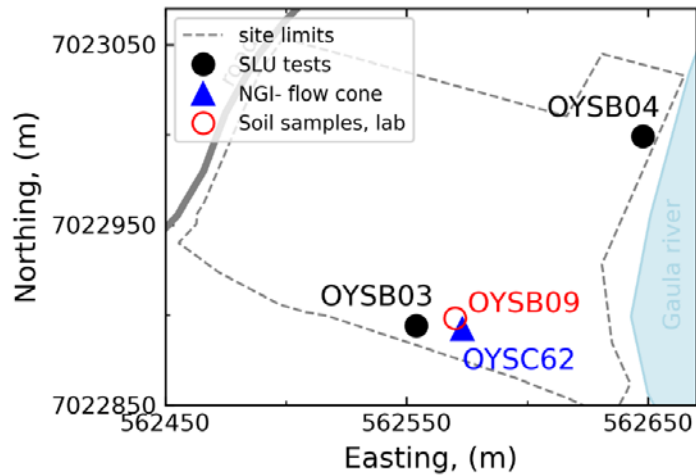


**Figure 19.** Locations of permeability tests.

Nine slug tests were performed in total, 4 on OYSB03 and 5 on OYSB04, in October 2017. A casing was installed in the ground with the use of a sonic drill rig. The top of the casing was 10–20 cm above terrain at the end of the installation. The casing was then filled with water, and the reducing water level inside the casing was logged together with time by a pressure logger installed inside the casing. The air pressure was also logged in order to correct the water pressure measurements. The tests were terminated when the water column inside the casing reached an assumed equilibrium. A sketch of the slug tests, together with the data obtained per depth, are shown in Figure 20. Tests results were assessed using the [25] interpretation procedures.

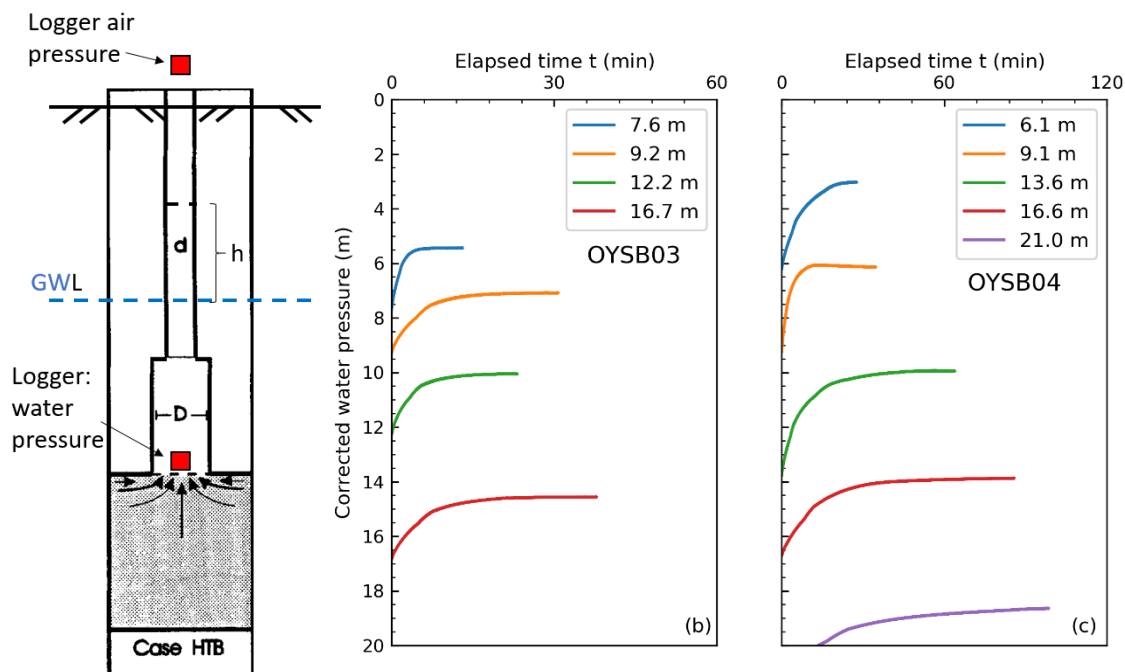


**Figure 20.** Slug tests: (a) testing scheme (b) tests on OYSB03, and (c) tests on OYSB04.

The NGI permeability flow cone, which has an add-on pumping system that allows water to flow into and out of the surrounding sediments while the CPTU test is performed, was also used at Øysand. Further details on how the flow cone results can be used to estimate the permeability with depth are given in [7].

Permeability estimates were also made based on grain size distribution curves using Hazen's empirical formulation for saturated sands shown in Eq 1 [26].

$$k = C_H D_{10}^2 \quad (1)$$

where  $k$  = permeability (cm/s),  $C_H$  = Hazen empirical coefficient, and  $D_{10}$  = particle size for which 10% of the soil is finer (cm).  $C_H$  was assumed as 100, as is most common in practice; however, values quoted in the literature can range from 1 to 1000. One laboratory constant head test was also conducted during a triaxial test, and slug tests have been carried out in the field. Figure 21 illustrates the cone resistance, soil behaviour type index and hydraulic conductivity from locations OYSC62 (black colour), OYSC60 (OYSB03—red colour) and OYSC09 (OYSB09—green colour).

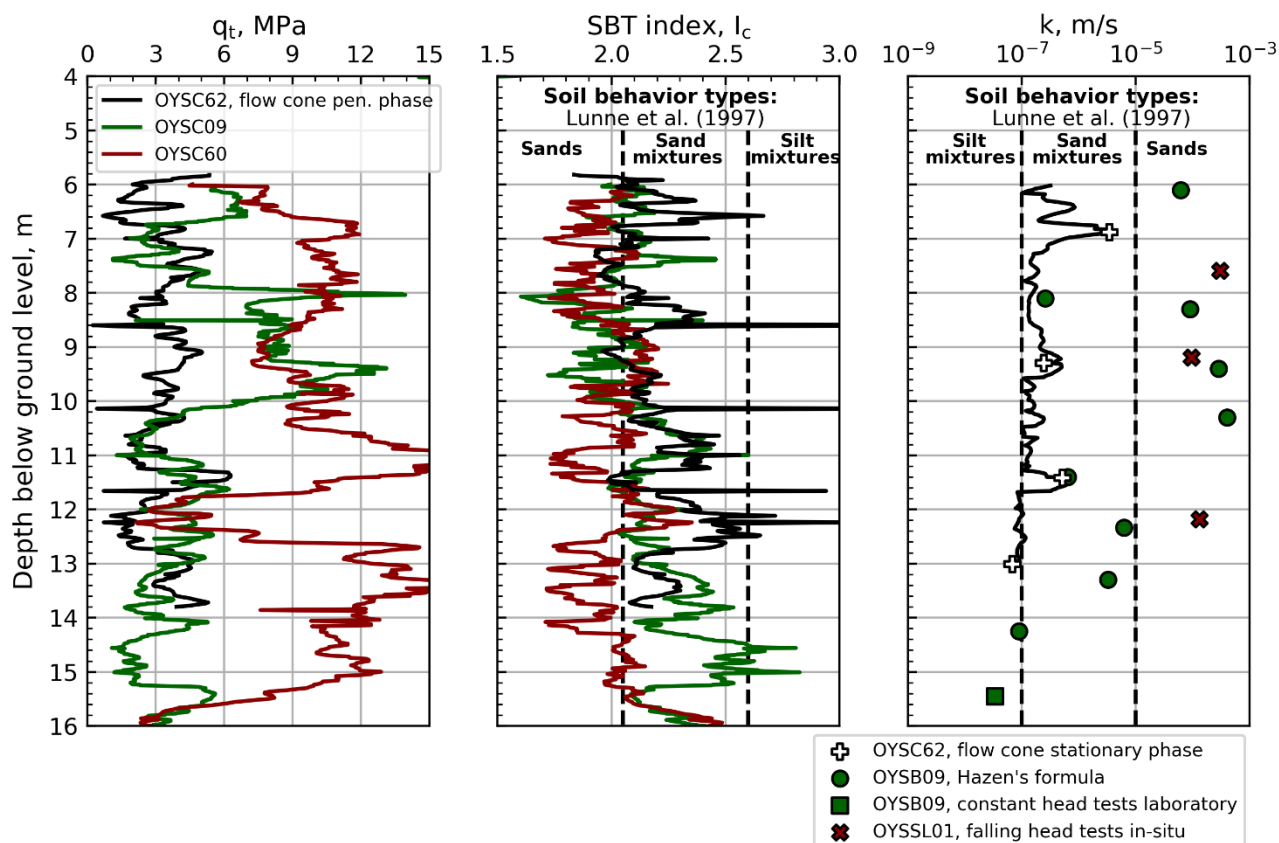


**Figure 21.** Cone resistance, soil behaviour type index and permeability from [7].

The cone resistance in Figure 21 suggests that there are large variations in soil behaviour for the locations at which the permeability testing was carried out. While the permeabilities from flow cone and Hazen's formula are comparable at 8 m and 11.4 m depth, there is considerable dispersion over the rest of the entire profile. Hydraulic conductivities from Hazen's formula generally range between  $10^{-7}$  m/s and  $10^{-3}$  i.e. four orders of magnitude, which may be expected given that the silt content varies between 0 and 70% (see borehole log in Figure 7). The slug test results generally fall far from the flow cone trends, but are in better agreement with Hazen's estimation. The differences between the flow cone and slug test results are mainly attributed to different soil conditions at the two test locations. Note that there are uncertainties related to the hydraulic conductivities measured at Øysand, hence the results should be treated with care.

### 7.6. Soil temperature

Soil temperature was measured between October 2017 and February 2018 (see Figure 22). A fluctuation in the order of about 8°C was observed in the top 8 m of soil. However, below a depth of 8 m, a constant temperature of about 6 degrees Celsius was recorded over the four month period. Knowledge of the temperature of soil layers at the site was important to assess the frost heave susceptibility of Øysand soils and for planning of the soil freezing campaign, which took place during April and May 2019.



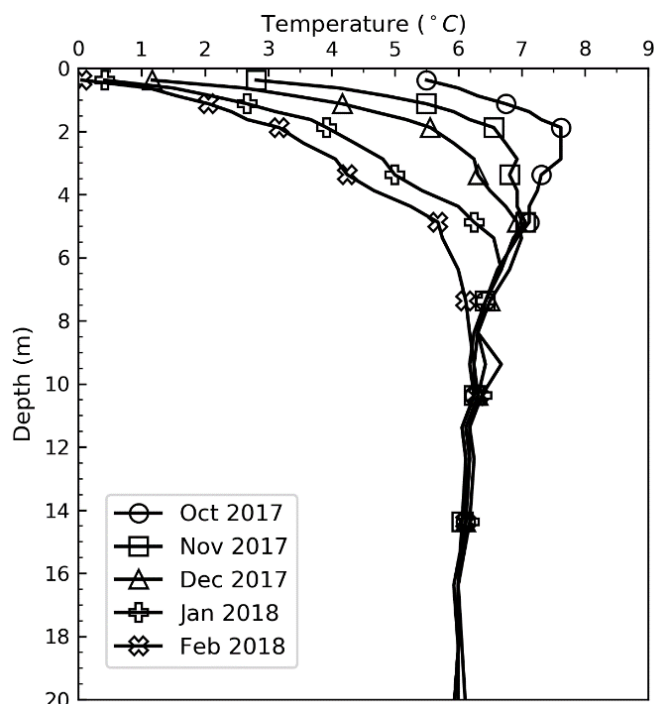


**Figure 22.** Temperature fluctuations between October 2017 and February 2018.

## 8. Advanced laboratory testing

### 8.1. Drained triaxial compression tests

A series of triaxial compression tests were performed on Øysand soil samples obtained with the Geonor push piston sampler at borehole OYSB09. These samples were obtained from the sandy silty soils of Unit II. When the triaxial tests were carried out under anisotropically-consolidated ( $K = 0.5$ , see Section 9.2) drained compression conditions (CADC), a mainly dilative response was observed. Peak angle of shearing resistance ( $\phi'_p$ ) values ranging from  $37^\circ$  to  $40^\circ$  were measured. The large strain data at the end of the test was used as a best estimation of critical states. The critical state angle of shearing resistance ( $\phi'_{cs}$ ) of the soil tested was about  $34^\circ$ . A plot showing the typical variation of the ratio of deviatoric stress ( $q$ ) to the mean effective stress ( $p'$ ) with axial strain for three samples collected from different depths is shown in Figure 23. A comparison between the CADC results obtained so far and correlations for estimating  $\phi'$  found in the literature is presented in Section 9.3.

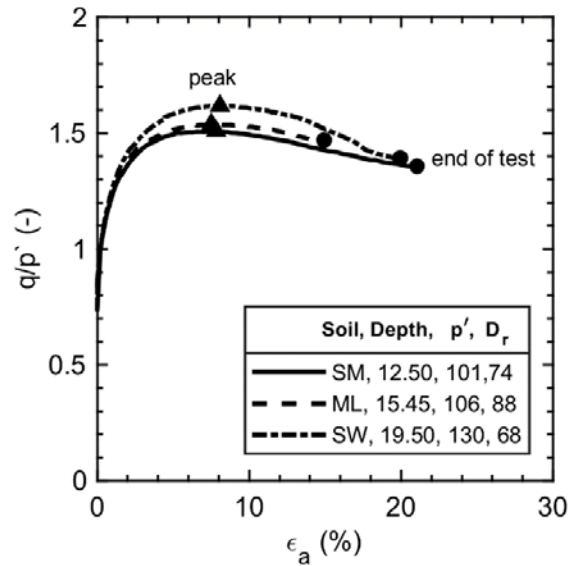


**Figure 23.** Triaxial test results on Øysand samples from OYSB09.

## 9. Engineering parameters

### 9.1. Overconsolidation ratio (OCR)

The overconsolidation ratio, OCR, is defined as the maximum past effective consolidation stress ( $\sigma'_p$ ) over the present effective overburden stress ( $\sigma'_{vo}$ ). For mechanically overconsolidated soils, where the only change has been the removal of overburden stress, this definition is appropriate. However, for cemented and/or aged soils the OCR may represent the ratio of the yield stress (or apparent overconsolidation) and the present effective overburden stress. Moreover, the yield stress will also depend on the direction and type of loading [27].

Assuming that 7 m of saturated soil was removed at the site by river erosion (groundwater assumed at surface level during erosion, refer to Figure 5), one can estimate the past maximal effective stress, also called the pre-consolidation stress, and OCR. The best estimate of  $\sigma'_p$  and OCR based on the most likely previous terrain level is shown in Figure 24. As shown on this figure, the OCR at about 2 m depth is estimated to be 2.0 and decrease to a value of 1.5 at a depth of 6 m and to a value of 1.2 at 20 m below the ground surface. OCR estimations depend on the assumption made with respect to the groundwater level during the erosion process.

OCR was estimated from CPTU tests using [28] unified-approach for evaluation of the yield stress. The equation presented by them is given below and it is considered as first-order estimation of the yield stress:

$$\sigma'_p = 0.33(q_t - \sigma_{vo})^{m'} \quad (2)$$

where,  $\sigma'_p$  = past effective consolidation stress,  $q_t$  = corrected cone resistance ( $q_t = q_c + u_2(1 - a)$ ) in kPa,  $\sigma_{vo}$  = vertical total stress in kPa, and  $m'$  is the fitting exponent =  $m' \approx 0.72$  for clean quartz to silica sand, 0.8 in silty sands, 0.85 in silts, 0.90 in organic and sensitive fine-grained soils, and  $m = 1.0$  in intact clays of low sensitivity.

OCR profiles based on the [28] equation are shown in Figure 24. The Øysand site is classified as normally consolidated (NC) or slightly overconsolidated (OC). Assuming an overburden pressure of 7 m of soil for calculating  $\sigma'_p$  can be used for calculating an upper boundary of OCR (see dashed lines profile in Figure 24).

Marchetti (1980) proposed the empirical equation  $OCR_{DMT} = (0.5 K_D)^{1.56}$  for estimating OCR (and  $K_0$ ) of NC-clays or soils of  $I_D < 1.2$  (Øysand sand has shown  $I_D$  values below about 2). There have been several other attempts for obtaining OCR-DMT correlations, e.g. [29–31]. However, according to [32], such correlations have been reported to be only of local applicability. According to [33], the estimation and the definition of OCR in sands is more difficult and a combination of CPTU and DMT readings ( $M_{DMT}/q_c$ ) may be the only way of obtaining an idea of OCR in sands. The following empirical correlation for Venice lagoon was proposed by [32].

$$OCR = 0.0344(M_{DMT}/q_c)^2 - 0.4174(M_{DMT}/q_c) + 2.2914 \quad (3)$$

where,  $M_{DMT}$  = constrained modulus, calculated by  $M_{DMT} = R_M E_D$ , and  $R_M = f(I_D, K_D)$ .

OCR results based on combined CPTU and DMT readings are plotted in Figure 24. Those OCR values fit with OCR estimated from CPTU tests.

## 9.2. Coefficient of earth pressure at rest, $K_0$ , and estimated in situ effective stresses

The coefficient of lateral earth pressure at rest is defined as:

$$K_0 = \frac{\sigma'_{ho}}{\sigma'_{vo}} \quad (4)$$

where,  $\sigma'_{ho}$  = effective horizontal stress and  $\sigma'_{vo}$  = effective vertical stress. Typical values of  $K_0$  reported in the literature are 0.5 for NC sands and 1.0 for OC sands.

Based on the simplified equation by [34,35] and to reflect the effect of OCR on  $K_0$ , a variation of  $K_0$  has been proposed by [36]:

$$K_0 = (1 - \sin\phi)OCR^{\sin\phi} \quad (5)$$

where  $\phi$  is assumed to be  $\phi'_{cs}$ , as proposed by [37] based on oedometer test on dense and loose sand.  $K_0$  values based on CPTU tests have been obtained using Eq 5, and OCR based on [31], results are show in Figure 24.

A multi-parameter approach similar to the OCR estimation has been proposed by [30] for calculating  $K_0$  from CPTU and DMT tests based on the calibration chamber data from [38] for Ticino and Hokksund sands. The equation for calculating  $K_0$  is

$$K_0 = 0.376 + 0.095K_D - D_3 \left( \frac{q_c}{\sigma'_v} \right) \quad (6)$$

where  $D_3$  = fitting parameter reported to be 0.0017 for calibration chamber data obtained from pluviated sand or 0.0046, which is a modified parameter to predict  $K_0$  for the natural Po river sand.  $D_3$  coefficient can be assumed to be 0.005 in sand deposited hundreds to thousands of years previously and 0.002 in freshly deposited sand [38]. A value of 0.005 was used to calculate the values of  $K_0$  presented in Figure 24. The representative profile of  $K_0$ , based on a past overburden pressure of 7 m of soil is also shown in dashed lines on that figure.

Figure 24c shows profiles of water pressure ( $u_w$ , based on piezometric data),  $\sigma_{tot,v}$  calculated from the unit weight values presented in Figure 7,  $\sigma'_v$  and  $\sigma'_h$  using the estimated  $K_0$  values estimated from Figure 24b. Note that OCR and  $K_0$  are not fixed values, they change with varying effective stresses, e.g. during seasonal variations of the groundwater as shown in Figure 4.

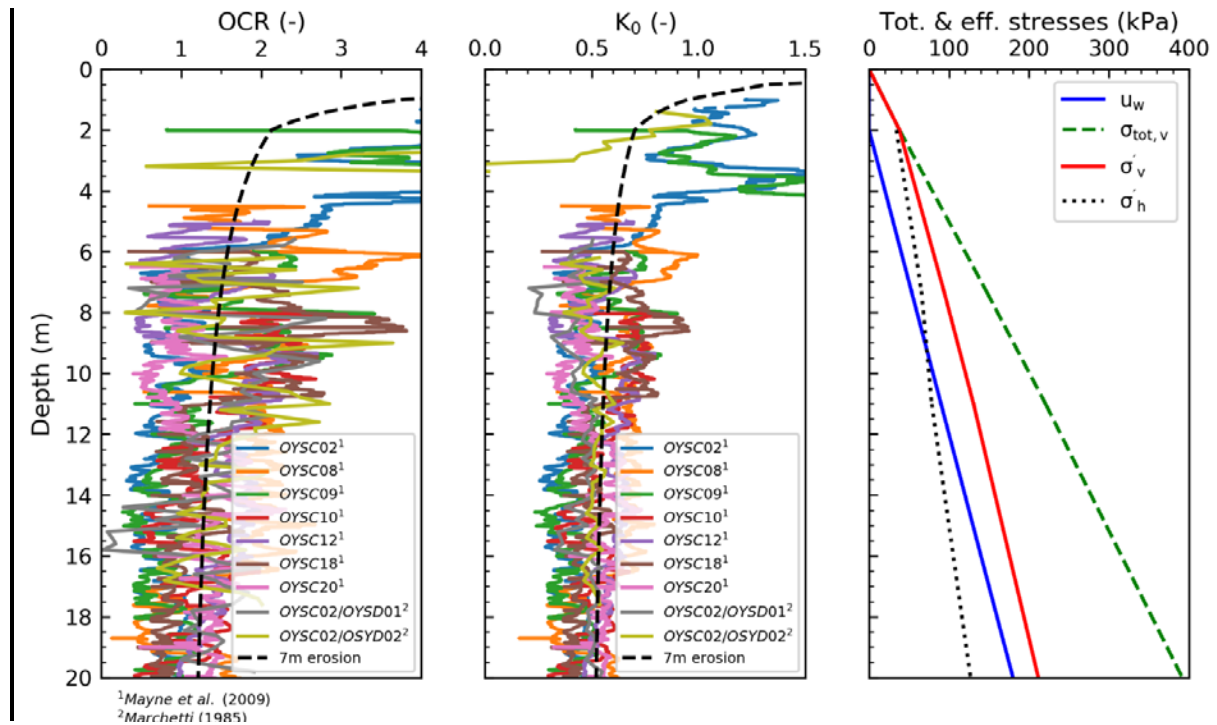


**Figure 24.** Estimation of: (a) OCR, (b)  $K_0$ , and effective stresses with depth.

### 9.3. Effective stress-strength parameters—field and laboratory testing

The peak and critical state angle of shearing resistance obtained from anisotropically consolidated drained ( $\phi'_p$ ,  $\phi'_{cs}$ ) triaxial compression tests (CADC) are compared against values estimated from empirical correlations from field tests available in the literature. CPTU, DMT and  $v_s$  were used to estimate *in situ* angles of shearing resistance.

For estimating the angle of shearing resistance based on CPTU data, the relationship between normalized cone resistance,  $Q_t$  and  $\phi'_p$  after [39] was chosen, see Eq (7). The relationship is valid for uncemented, unaged, freshly deposited sand, moderately compressible, predominately quartz sands.

$$\phi'_{p,CPT} = 17.7^\circ + 11.0^\circ \times \log(q_{t1}) \quad (7)$$

where,  $q_{t1}$  = normalized cone resistance ( $q_{t1} = q_t / (p_a \cdot \sigma'_{vo})^{0.5}$ ).

An equation for estimating a so-called safe (or lower bound) angle of shearing resistance,  $\phi'_{safe,DMT}$  based on DMT data has been proposed by [40]. The equation is valid for unaged, uncemented sands.  $\phi'_{safe,DMT}$  is calculated from the intermediate parameter  $K_D$ , see Eq 8.

$$\phi'_{safe,DMT} = 28 + 14.6 \log(K_D) - 2.1 \log(K_D)^2 \quad (8)$$

where,  $K_D$  = Horizontal stress index ( $K_D = (p_0 - u_0)/\sigma'_{vo}$ ),  $p_0$  = DMT first correct reading.

Since  $v_s$  is more sensitive to OCR,  $D_r$  and the sand's microstructural features, e.g. cementation, bonding and ageing, an estimation of  $\phi'_p$  from  $v_s$  was made. The following correlation for estimating of  $\phi'_p$  on sands based on  $v_{s1}$  has been proposed by [41].

$$\phi_{p,v_{s1}} = 3.9(v_{s1})^{0.44} \quad (9)$$

where,  $\phi'_p$  = peak angle of shearing resistance and  $v_{s1}$  = normalized shear wave velocity ( $v_{s1} = v_s/(p_a/\sigma'_{vo})^{0.25}$ ),  $p_a$  = atmospheric pressure = 100 kPa, and  $\sigma'_{vo}$  = vertical effective stress.

Estimated values of  $\phi'_p$  based on CPTU, DMT and  $v_s$ , in comparison with laboratory data from CADC tests, are shown in Figure 25. In general, reasonable estimations of  $\phi'_p$  based on CPTU and  $v_s$  were obtained. The DMT correlation estimates  $\phi'_{safe, DMT}$  values, somewhat lower than  $\phi'_{cs} = 34^\circ$  from triaxial tests. Note that peak angles of shearing resistance depend on the sand state, which may have been affected by the sampling process. Hence, the currently presented laboratory values of  $\phi'_p$  should be taken with care. The level of disturbance of samples obtained with a piston sampler can be significant in sands.

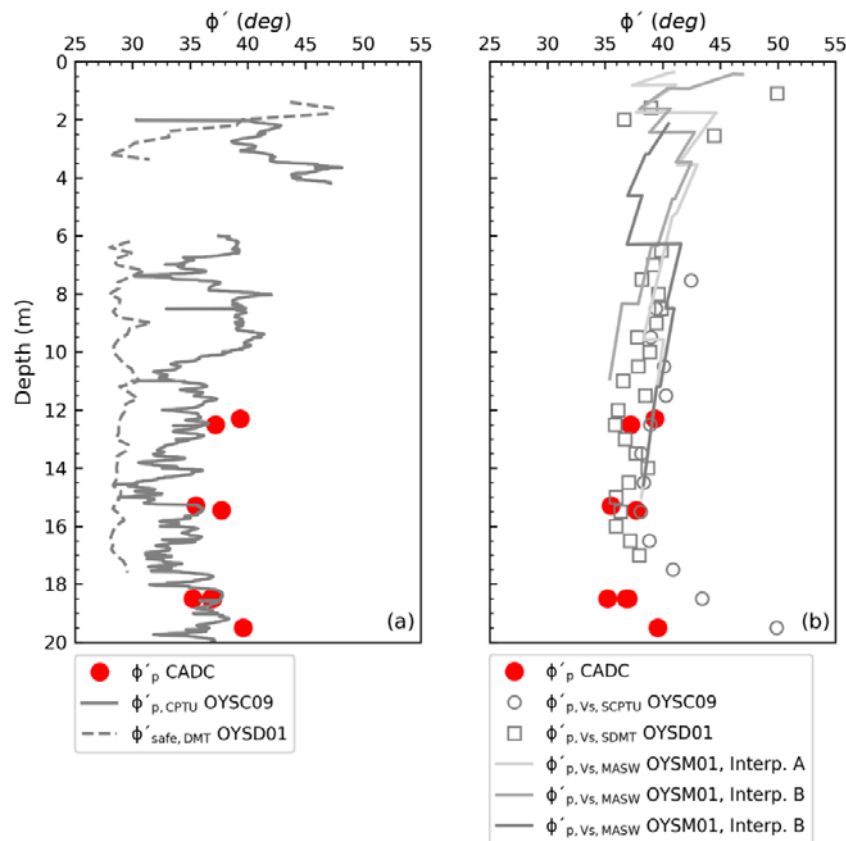


**Figure 25.** Measured and interpreted angles of shearing resistance (a) triaxial tests, CPTU and DMT, and (b) triaxial tests and  $v_s$ .



## 10. Further geotechnical characterisation considerations

### 10.1. Impact of cone penetrometer type on CPTU results

CPTUs from several manufacturers were tested at Øysand, including Geomil, A.P.van den Berg, Pagani, Environmental Mechanics (Envi) and Geotech AB CPTU cones. The 7 cones types used are 10 cm<sup>2</sup> compression cones with 150 cm<sup>2</sup> friction sleeves and the pore pressure transducer located in the  $u_2$  position. The CPTU tests were carried out following [20]. CPTUs were performed very close to each other, to avoid as much as possible the inherent soil variability. Results of different cones types are presented in Figure 26. Details of the cones type used (geometry, calibrations, filter materials, saturation fluids used, etc.) are found in [42]. As seen in Figure 26,  $q_t$  can vary about 2 MPa,  $f_s$  up to 0.08 MPa and  $u_2$  up to 0.2 MPa depending on the CPTU type used. In general, the smallest variability is observed for  $u_2$ . Hence,  $u_2$  is the most reliable parameter. The largest variation is observed in  $f_s$ , making this parameter the least reliable. The research showed also the importance of good procedures for taking zero readings and also taking into account temperature effects on CPTU readings.

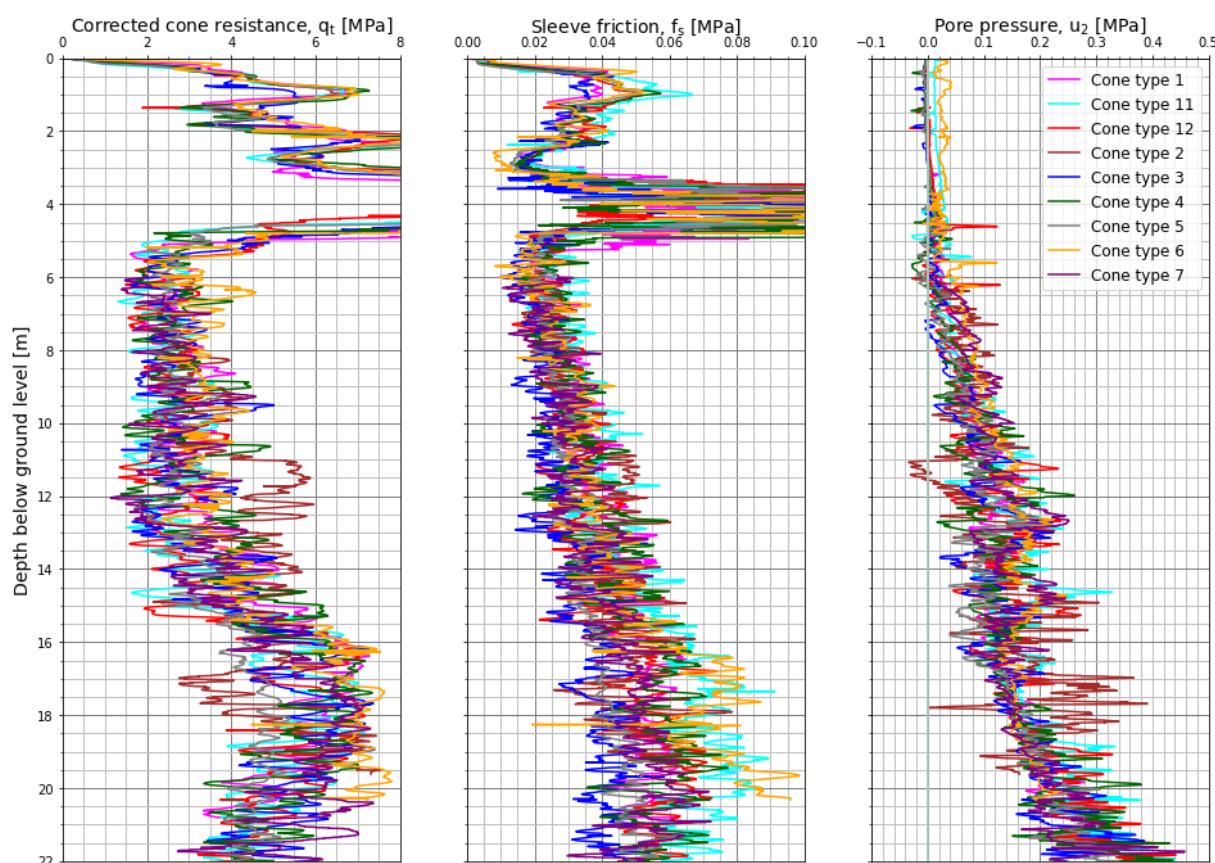


**Figure 26.** Variation of CPTU readings depending on cone type: (a)  $q_c$ , (b)  $f_s$ , (c)  $u_2$  with depth.

### 10.2. Sample quality research in progress

An evaluation of sample quality is ongoing for the Øysand site. As described in Table 1 soil sampling has been and will be done using several techniques. Those techniques are: (i) Geonor 54 mm fixed piston composite sampler, (ii) 72 mm thin walled fixed piston sampler, (iii) Gel-Push sampler (without success so far, only two samples obtained) and (iv) soil freezing (see Figure 27). Results from the ground freezing investigation are in progress and will be reported subsequently. Reconstituted specimens will also be tested, and the results of “intact” and reconstituted advanced tests will be compared.



**Figure 27.** Installation of soil freezing pipes at Øysand in March 2019.

### 10.3. Frost heave susceptibility of Unit II sandy/silty soils

Since a ground freezing campaign is being performed at Øysand, it was necessary to assess the frost susceptibility of the soils to be frozen. Sandy silty mixtures at Øysand are classified as frost susceptible. The main Øysand soil types will be tested in the one-dimensional freezing cell to determine if they are susceptible to heave expansion. The cell used was developed by the Korean Institute of Civil Engineering and Building Technology (KICT) and modified at NGI. Details of the cell development and its components are found in [43]. An image of the modified setup used is shown in Figure 28. Preliminary results have shown that sandy soil layers at Øysand are not frost susceptible, hence the ground freezing technique can be used for stabilization prior to sampling of those soils.

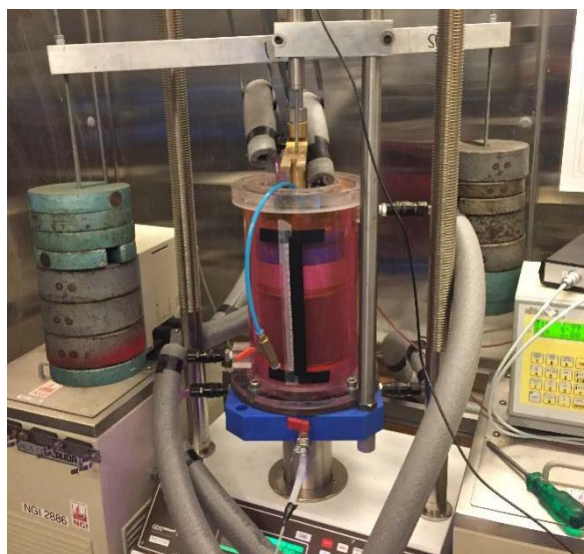


**Figure 28.** Frost susceptibility test on Øysand soils.

## 11. Summary and conclusions

This paper presents an overview of the geophysical and geotechnical characterisation of the sandy silty soils of the Øysand research site. State-of-the-practice and state-of-the-art *in situ* characterisation techniques have been used to investigate stratigraphy and to derive engineering parameters. Shear strength and stiffness parameters have been presented from both *in situ* and laboratory testing approaches. Examples of engineering characterisation problems currently being investigated at Øysand have also been discussed. Insights obtained so far include:

- The fluvial and deltaic deposits encountered show lateral (mainly north to south) and vertical variations. The main layers identified comprise: a gravelly sand layer encountered down to a maximum of 10 m depth over sandy silty soils that were proven down to 20 m depth. The bedrock depth was not established, but is thought to exceed 80 m.
- Comprehensive field and laboratory testing programmes have been carried out on the site. The geotechnical tools include total sounding, seismic penetrometer, piezometer, seismic dilatometer, multi-channel analysis of surface waves, slug tests and temperature measurements. Laboratory testing include index and advanced laboratory testing.
- The Øysand site soils are normally-to-lightly overconsolidated; the critical state angle of shearing resistance of the sand layer at OYSB09 is assumed to be about 34°. A strongly dilative response was observed during drained laboratory triaxial compression tests on tubed 54 mm diameter Geonor push piston samples. Peak angles of shearing resistance of up to 40° were measured in these tests.  $G_{\max}$  values varied between about 50 MPa and 100 MPa depending on the *in situ* tool used and depth. Soil permeability measurements ranged over several orders of magnitude. The determination of  $k$  is highly method dependent. At Øysand, permeability ranges between  $10^{-7}$  m/s and  $10^{-3}$  m/s. Temperature fluctuations of the upper 8 m have been recorded. Below that depth, a constant temperature of 6 °C is observed.
- Some geotechnical engineering characterisation problems under investigation at Øysand have been briefly introduced. Those problems are related to (i) the impact of using different CPTU

types, (ii) the assessment of sample quality by sampling soil using different state-of-the-practice and state-of-the-art techniques, and (iii) determining the frost susceptibility of Øysand soils.

## Acknowledgments

The authors would like to thank Tom Lunne for his support and the Research Council of Norway for their generous infrastructure grant to establish the five Norwegian GeoTest Sites for research (Grant No. 245650/F50). The authors acknowledge the significant contributions from Pagani, Geomil Equipment, In situ SI, the Norwegian Public Roads Administration, Geological Survey of Norway and colleagues at NGI Field Investigations (Kristoffer Kåsin, Pål Kristian Karstensen, Magnus Hunemo, Rolf Ove Karlsen and Håvard Saur) and NGI Geosurveys (Helge Smebye and Sara Bazin). The work presented in this paper is part of the PhD research of the leading author at Imperial College London, funded by the Norwegian Geotechnical Institute and the Norwegian Research Council.

## Conflict of interest

All authors declare no conflicts of interest in this paper.

## References

1. L'Heureux JS, Lunne T, Lacasse S, et al. (2017) Norway's National GeoTest Site Research Infrastructure (NGTS). In Proceedings of the 19th International Conference on Soil Mechanics and Geotechnical Engineering. Seoul.
2. Blaker Ø, Carroll R, Paniagua P, et al. (2019) Halden research site: geotechnical characterization of a post glacial silt. *AIMS Geosci* 5: 184–234.
3. Gundersen AS, Hansen RC, Lunne T, et al. (2019) Characterization and engineering properties of the NGTS Onsøy soft clay site. *AIMS Geosci* 5: 665–703.
4. L'Heureux JS, Lindgård A, Emdal A (2019) The Tiller-Flotten research site: Geotechnical characterization of a very sensitive clay deposit. *AIMS Geosci* 5 [In press].
5. Gilbert GL, Instanes A, Sinityn AO, et al. (2019) Characterization of the NGTS permafrost sites: Longyearbyen, Svalbard. *AIMS Geosci* 5 [In press].
6. Salgado R (2008) *The engineering of foundations*. McGraw-Hill New York.
7. Gundersen AS, Carotenuto P, Lunne T, et al. (2019) Measurements of hydraulic soil properties at NGTS sand site using a newly-developed in-situ tool. *AIMS Geosci* 5 [In press].
8. Reite AJ (1994) *Weischelian and Holocene geology of Sør-Trøndelag and adjacent parts of Nord-Trøndelag county, Central Norway*. Norges Geol undersøkelse-Bulletin, 1–30.
9. Reite AJ, Sveian H, Erichsen E (1999) *Trondheim fra istid til nåtid—landskapshistorie og løsmasser*. Norges Geol undersøkelse Gråsteinen 5: 40.
10. Wolff FC (1979) *Beskrivelse til de berggrunnsgeologiske kart Trond-heim og Østersund 1:250,000*. Norges Geol undersøkelse 353: 76.

11. Gundersen AS, Quinteros S, L'Heureux JS, et al. (2018) Soil classification of NGTS sand site (Øysand, Norway) based on CPTU, DMT and laboratory results. In 4th International Symposium on Cone Penetration Testing. CPT18, 323–328.
12. Cosentini RM, Della Vecchia A G, Foti S, et al. (2012) Estimation of the hydraulic parameters of unsaturated samples by electrical resistivity tomography. *Géotechnique* 62: 583–594.
13. Lunne T, Robertson PK, Powell JJM (1997) *Cone Penetration Testing in Geotechnical Practice*. New York.
14. ASTM (2017) D2487-17 Standard Practice for Classification of Soils for Engineering Purposes (Unified Soil Classification System).
15. Powers MC (1953) A new roundness scale for sedimentary particles. *J Sediment Petrol* 23: 117–119.
16. NS 8012 (1982) Geoteknisk prøving. Laboriemetoder. Korndensitet. Standard Norge, Lysaker.
17. Lunne T, Knudsen S, Blaker Ø, et al. (2019) Methods used to determine maximum and minimum dry unit weight of sand. Is there a need for a new standard? *Can Geotech J* 56: 536–553.
18. Jamiolkowski M, Lo Presti DCF, Manassero M (2003) Evaluation of relative density and shear strength of sands from CPT and DMT. In Germaine JT, Sheahan TC, Whitman RV (eds), *Soil behavior and soft ground construction*, ASCE GSP, 201–238.
19. NGF (2018) Guidelines for performing total sounding tests (In Norwegian: Veiledning for utførelse av totalsondering). Norwegian Geotechnical Society, Norway.
20. ISO 22476-1 (2012) Geotechnical investigation and testing—Field testing—Part 1: Electrical cone and piezocone penetration test.
21. ISO 22476-11 (2017) Geotechnical investigation and testing—Field testing—Part 11: Flat dilatometer test
22. Marchetti S (1980) In situ tests by flat dilatometer. *J Geotech Geoenviron Eng* 106: 299–321.
23. Kuwano R, Jardine RJ (2002) On the applicability of cross-anisotropic elasticity to granular materials at very small strains. *Géotechnique* 52: 727–750.
24. Jardine RJ (2013) Advanced laboratory testing in research and practice. 2nd Bishop Lecture. Proc. ICSMGE. Presses des Ponts, Paris, 1: 35–55.
25. Demir Z, Narasimhan TN (1994) Improved Interpretation of Hvorslev Tests. *J Hydraul Eng* 120: 477–494.
26. Hazen A (1911) Discussion of Dams on sand foundations. *Trans Am Soc Civ Eng* 73: 199–203.
27. Robertson PK, Cabal KL (2015) Guide to Cone Penetration Testing for Geotechnical Engineering, 6th Editio. Gregg Drilling & Testing Inc., California.
28. Mayne PW (2009) *Geoengineering Design Using the Cone Penetration Test*. ConeTec Inc., Richmond, BC, Canada.
29. Schmertmann JH (1983) Revised procedure for calculating  $K_0$  and OCR from DMT's with  $I_d > 1.2$  and which incorporates the penetration force measurement to permit calculating the plane strain friction angle. In Proc. of the 1st Int. Conf. on the Flat Dilatometer. Gainesville, FL.
30. Marchetti S (1985) On the field determination of  $K_0$  in sand. In 11th Int. Conf. on Soil Mech. and Found. Eng. Panel Presentation, Balkema Pub., Rotterdam, 5: 2667–2672.

31. Mayne P, Coop MR, Springman S, et al. (2009) Geomaterial behavior and testing. In Proc. 17th International Conference on Soil Mechanics and Geotechnical Engineering. Alexandria, Egypt, 4: 1–96.
32. Monaco P, Amoroso S, Marchetti S, et al. (2014) Overconsolidation and Stiffness of Venice Lagoon Sands and Silts from SDMT and CPTU. *J Geotech Geoenviron Eng* 140: 215–227.
33. Marchetti S, Monaco P, Totani G, et al. (2001) The Flat Dilatometer Test (DMT) in Soil Investigations. International Conference on Insitu Measurement of Soil Properties and Case Histories (Insitu 2001). Parahyangan Catholic University, 95–131.
34. Jaky J (1944) The coefficient of earth pressure at rest. In Hungarian (A nyugalmi nyomás tenyezője). *J Soc Hung Eng Arch* (MagyarMernok es Egit Kozlonye), 355–358.
35. Jaky J (1948) Pressure in silos. In: Proc. 2nd Int. Conf. on SoilMechanics and Foundation Engineering. Rotterdam, The Netherland, 1: 103–110.
36. Mayne P, Kulhawy FH (1982) Ko-OCR relationships in soil. *J Soil Mecha Found Div* 108: 851–872.
37. Lee J, Park D, Kyung D, et al. (2003) Effect of particle characteristics on Ko behaviour of granular materials. In Proceedings of the 18th International Conference on Soil Mechanics and Geotechnical Engineering, Paris, 337–380.
38. Baldi G (1986) Interpretation of CPTs and CPTUs, 2nd part: drained penetration of sands. In Proceedings of the Fourth International Geotechnical Seminar. Singapore, 143–156.
39. Mayne PW (2014) KN2: Interpretation of geotechnical parameters from seismic piezocone tests. In: Robertson PK, Cabal KL (eds), Proceedings, 3rd International Symposium on Cone Penetration Testing (CPT'14, Las Vegas), ISSMGE Technical Committee TC 102, 47–73.
40. Marchetti S (1997) The Flat Dilatometer: Design Applications. In Third Geotechnical Engineering Conference Cairo University. Cairo, 421–448.
41. Uzielli M, Mayne PW, Cassidy M, et al. (2013) Probabilistic assignment of design strength for sands from in-situ testing data. In Advances in Soil Mechanics & Geotechnical Engineering (series), IOS-Millpress, Amsterdam, 1: 214–227.
42. NGI (2018) Impact of cone penetrometer type on CPTU results at 4 NGTS Sites. Silt, Soft Clay, Sand, and Quick Clay. Report No. 20160154-21-R. Oslo, Norway.
43. Jin HW, Lee J, Ryu BH, et al. (2019) Simple frost heave testing method using a temperature-controllable cell. *Cold Reg Sci Technol* 157: 119–132.

